Chinese Chemical Letters 33 (2022) 2301–2315

Contents lists available at ScienceDirect

Chinese Chemical Letters

journal homepage: www.elsevier.com/locate/cclet

Complex coordinated functional groups: A great genes for nonlinear optical materials

Weikang Wang[a], Dajiang Mei[a,c,*], Shaoguo Wen[a], Jian Wang[b], Yuandong Wu[a]

[a] College of Chemistry and Chemical Engineering, Shanghai University of Engineering Science, Shanghai 201620, China
[b] Department of Chemistry and Biochemistry, Wichita State University, Wichita, KS 67260, United States
[c] State Key Laboratory of Structural Chemistry, Fujian Institute of Research on the Structure of Matter, Chinese Academy of Sciences, Fuzhou 350002, China

ARTICLE INFO

Article history:
Received 13 September 2021
Revised 21 October 2021
Accepted 29 November 2021
Available online 4 December 2021

Keywords:
Complex coordinated
Nonlinear optical
Second harmonic generation
Optical band gap
Structure-performance relationship

ABSTRACT

Complex coordinated functional groups [MA_xB_y] (M = Central coordination element; A, B = P, O, S, Se, F, Cl, Br or I) are composed of different types of anions A, B jointly linked to the same central cation M, which are in high potential to tune the physical properties of materials, *e.g.*, second-order susceptibility, energy gaps and birefringence. Recently, Compound containing complex coordinated functional groups have attracted great attention in the nonlinear optical (NLO) field and a large number of this type crystals exhibit promising NLO performance. However, the inherent relationship between ionic group structure and optical properties of complex coordinated NLO materials have not been systematically studied. This article systematically summarizes complex coordinated NLO materials in recent five years from the perspective of the internal relationship between crystal structure and optical properties. In addition, we propose the ideal combination and arrangement modes for structural building units, and also reveal the influence of complex coordinated functional groups [MA_xB_y] toward the NLO response, optical band gap and phase matching ability of complex coordinated NLO materials.

1. Introduction

Nonlinear optical (NLO) crystals can generate tunable laser beams from deep ultraviolet (DUV, wavelength less than 200 nm) to mid IR (MIR, wavelength between 3 μm and 30 μm) *via* frequency conversion technology, thus plays an important role in optoelectronic and laser technology [1–14]. Researchers have been dedicated to explore NLO crystals with good performance since Franken *et al.* discovered second harmonic generation phenomenon in quartz crystal in 1961 [15]. In the past few decades, many NLO crystals with comprehensively excellent properties have emerged, such as β-BaB_2O_4 (β-BBO) [16], LiB_3O_5 (LBO) [17], $LiNbO_3$ (LN) [18], KH_2PO_4 (KDP) [19] and $KTiOPO_4$ (KTP) [20]. With the extensive application of laser from the 21st century, the demand for DUV and MIR laser keeps increasing [21–25]. However, the commercialized crystals in the DUV and MIR region cannot meet the practical needs due to the lack of comprehensive performances [26–29]. The prerequisites of the ideal NLO crystal in these two important wavelength regions are large second harmonic generation (SHG) coefficient d_{ij}, suitable birefringence value Δn and wide optical band gap E_g [30,31]. Large SHG coefficient d_{ij} corresponds to high frequency conversion efficiency, and suitable birefringence value Δn can ensure the phase matching output [32–34]. Wide optical band gap E_g corresponds to short ultraviolet cut-off edge and large laser damage threshold [35].

According to the anion group and functional moieties theory, the optical properties of the compounds are mainly affected by the anion functional groups in the structure [36–38]. Keeping a good balance among d_{ij}, Δn and E_g is not easy for NLO crystals with only one anionic functional group [39]. Rational combination of various anionic functional groups is critical to obtain the ideal NLO crystals. In the last few years, different research groups have systematically summarized the NLO materials with mixed anion. For example, De Yoreo *et al.* comprehensively reviewed the crystal chemistry and optical properties of metal halide borate NLO materials, according to the arrangement of anionic groups (0D clusters, 1D chain, 2D layer, 3D network) [19]. Pan *et al.* specifically analyzed the crystal chemistry and optical properties of the mixed anion NLO materials [39]. Li *et al.* summarized different types of IR mixed anion NLO inorganic compounds from the perspective of structure-property relationship [40].

* Corresponding author at: College of Chemistry and Chemical Engineering, Shanghai University of Engineering Science, Shanghai 201620, China.
E-mail address: meidajiang718@pku.edu.cn (D. Mei).

https://doi.org/10.1016/j.cclet.2021.11.089
1001-8417/

Inorganic salts containing two or more anions or anionic groups are normally defined as mixed anion compounds. For example, two type ions Cl^- and S^{2-} exist in the structure of salt sulfide halide compounds $[K_3Cl][Ga_3PS_8]$ [41]. There are two single anion functional groups $[IO_3]$ and $[NO_3]$ in iodate nitrates $Sc(IO_3)_2(NO_3)$ [42]. It should be noted that the compounds above are composed of different types of anions or anionic groups. Different from the traditional mixed anion compounds, the different anions A and B of $[MA_xB_y]$ groups in complex coordinated crystals jointly link to the same central atom M [43]. Complex coordinated functional groups exhibit superior propertiesthan the single-anion group from the following aspects: (1) The structure of mixed anion group $[MA_xB_y]$ has a stronger distortion and polarity, which is conducive to a strong SHG effect. (2) Due to different size and electronic properties of A and B anions, the mixed anion group $[MA_xB_y]$ has stronger anisotropy and large birefringence values, which is conducive to the appropriate phase matching ability. (3) In the DUV nonlinear optics field, the compounds containing mixed anion group produced by the introduction of halogen element with strong electronegativity, *e.g.*, F and oxygen in $[B/PO_4]$ have a wider DUV transparent region and also strong SHG effects and a suitable birefringence value. (4) In the field of IR NLO region, the compounds containing $[MO_xS_y]$ gene containing O and S can have large band gap and strong NLO effect [43–46]. The mixed anion functional group $[MA_xB_y]$ has been proven to be superior NLO active units, and the compounds containing this group are more likely to keep a good balance among three key property parameters (d_{ij}, Δn and E_g) [27,40]. For example, the well-performed DUV NLO crystal $KBe_2BO_3F_2$(KBBF) contains the mixed anion group $[BeO_3F]$ [47,48]. Moreover, the strongly polarized mixed anion group $[SbOS_4]$ has been recognized as the origin of the strong SHG effect in the new MIR NLO crystal $Sr_6Cd_2Sb_6O_7S_{10}$ [46]. Since 2017, complex coordinated NLO materials have attracted great attention in the NLO field. Different research groups have designed and synthesized a large number of NLO optical crystals with mixed anion groups, which have potential to become candidates for the next generation of DUV and MIR NLO crystals. For example, AB_4O_6F (A = Rb, Cs, K, Na, NH_4) series [42,49–51], $A(B_5O_7)F_3$ (A = Sr, Ca, Pb) series [52–54], $Ba_3Mg_3(BO_3)_3F_3$ [55], $CsAlB_3O_6F$ [56], γ-Be_2BO_3F [57], $C(NH_2)_3SO_3F$ [58], $Ba_2NaP_2O_7Cl$ [59], $CsSiP_2O_7F$ [60], $NaNH_4PO_3F{\cdot}H_2O$ [61], have short ultraviolet cut-off edges and strong SHG effect, thus are regarded as potential source of DUV NLO crystals. $K_5(W_3O_9F_4)(IO_3)$ [62], $BiIO_3F$ [63], $(NH_4)Bi_2(IO_3)_2F_5$ [64], $CsVO_2F(IO_3)$ [65], $K_2Bi_2(SeO_3)_3F_2$ [66], $Pb_2GaF_2(SeO_3)_2Cl$ [67], $Pb_{13}O_6Cl_9Br_5$ [68] and $M^{II}{}_3PnI_3$ (M^{II} = Zn, Cd; Pn = P, As) [69], *etc.*, have a wide MIR transparent area, which can achieve a good balance between a wide E_g and a large d_{ij}, regarded as a potential candidate of MIR NLO crystals. The difference between traditional complex coordinated compounds and those with complex coordinated groups as structural building units (SBUs) are still not clear, especially systematic summary of how complex coordinated functional groups $[MA_xB_y]$ influence on the optical properties of NLO crystal materials.

This article focuses on complex coordinated NLO materials in recent five years. The preparation methods, crystal structure, and optical properties of this type NLO crystals are comprehensively reviewed. The regulation law of multiple critical properties (SHG effect, phasemaching capability and band gap) by the permutation pattern of the complex coordinated functional group $[MA_xB_y]$ was highlighted. *Via* the structure-performance analysis of the NLO complex coordinated materials, the ideal combination and arrangement modes of the anion group of UV/DUV and MIR NLO complex coordinated crystals are proposed, respectively. We hope that this article can help future research minimize time-consuming "trial and error" and provide some insights on the design and synthesis of next-generation complex coordinated NLO crystals.

2. IR complex coordinated NLO materials

In the field of infrared (IR) nonlinear optics, the common single-anion NLO active units (NAUs) consist of tri-coordinated and tetra-coordinated groups. Tri-coordinated groups play a key role in NLO response, and exhibit large microscopic SHG effects and good optical anisotropy [70–72]. Tetrahedron-based sulfides have been widely used in the research on IR NLO crystals due to their spacious IR transparent region and good balance between E_g and d_{ij} [73]. In the last few years, a number of research groups have combined these single-anion units with mixed anion groups to design and synthesize a series of new IR NLO materials. In this part, some representative complex coordinated compounds are presented and the relationship between crystal structure and optical properties of this type compounds are summarized in detail (Table 1). According to the types of anions, the IR NLO crystals containing single anions and mixed anions as SBUs can be divided into: (1) $[MA_xB_y]$ and $[IO_3]$ as SBUs; (2) $[MA_xB_y]$ and $[Se/TeO_3]$ as SBUs; (3) $[MA_xB_y]$ and $[MS_4]$ as SBUs. In addition, another type IR complex coordinated NLO materials contain only mixed-anion $[MA_xB_y]$. In the field of IR nonlinear optics, this type of compound mainly includes the following three groups: (1) PbO-$PbCl_2$-$PbBr_2$, PbO-$PbCl_2$-PbI_2 series of IR NLO crystals containing O-Pb-X complex coordinated groups; (2) $M^{II}{}_3PnI_3$ containing $[MPn_3I]$ mixed anion (M^{II} = Zn, Cd; Pn = P, As) series pnictides; (3) oxychalcogenides.

2.1. $[MA_xB_y]$ and $[IO_3]$ as NLO active units

The iodates with the lone pair electron benefit the formation of the NCS structure required by the compound for the SHG response. $[IO_3]$ group has received extensive attention in NLO region due to their wide IR transparent region [74]. Recently, Mao, Ye, Poeppelmeier and other research groups combined the $[IO_3]$ group with the mixed anion group $[MA_xB_y]$ to design and synthesize a series of IR NLO crystals with excellent performance, such as $Ba_2[GaF_4(IO_3)_2](IO_3)$ [75], $(NH_4)Bi_2(IO_3)_2F_5$ [64], $Ba_2[VO_2F_2(IO_3)_2]IO_3$ [76]. This section summarizes this type of NLO crystal from the perspective of the structure-performance relationship and anionic group structure dimensions from 0D to 3D.

2.1.1. 0D cluster formed by $[MA_xB_y]$ and $[IO_3]$ anionic groups

$Ba_2[GaF_4(IO_3)_2](IO_3)$ polymorphs are representative compounds of this type iodates. Mao *et al.* obtained colorless and transparent α-$Ba_2[GaF_4(IO_3)_2](IO_3)$ and β-$Ba_2[GaF_4(IO_3)_2](IO_3)$ [75] on the basis of $Ba_2[VO_2F_2(IO_3)_2](IO_3)$ [76] by chemical substitution. They have a similar crystal structure. Taking α-$Ba_2[GaF_4(IO_3)_2](IO_3)$ as an example, its structure is composed of one mix-anion $[GaF_4O_2]$ group and two $[IO_3]^-$ groups to form OD isolation molecular structure (Fig. 1a). Ba^{2+} is trapped in molecular voids to maintain charge balance. Both of them exhibit wide transparent areas of 0.26–12.5 μm and 0.28–12.9 μm, respectively. The powder test shows that both of them have phase matching ability and strong SHG response of 6 times that of KDP (d_{36} = 0.38 pm/V) under 1064 nm laser irradiation. Optical experiments revealed that they have a large E_g: 4.61 and 4.35 eV. The theoretical analysis of partial densities of states (PDOS) shows that the valence bands (VBs) maximum is occupied by O 2p orbitals, while the conduction bands (CBs) minimum is contributed by O 2p and I 5p orbitals, which indicates that its optical properties are mainly dominated by $[IO_3]$ groups. The 2p orbital of F is above top of the VBs, which indicates that the mix-anion $[GaF_4O_2]$ group contribute the large energy band gap.

Table 1
Optical properties of IR complex coordinated NLO crystals.

Compounds	SG	SBUs	SHG effect	E_g (eV)	PM/NPM	Ref.
α-$Ba_2[GaF_4(IO_3)_2](IO_3)$	$Pna2_1$	$[GaO_2F_4]$, $[IO_3]$	6.0 × KDP	4.61	PM	[75]
β-$Ba_2[GaF_4(IO_3)_2](IO_3)$	$Pna2_1$	$[GaO_2F_4]$, $[IO_3]$	6.0 × KDP	4.35	PM	[75]
α-$Ba_2[VO_2F_2(IO_3)_2]IO_3$	$Pna2_1$	$[VO_4F_2]$, $[IO_3]$	9 × KDP	2.56	PM	[76]
β-$Ba_2[VO_2F_2(IO_3)_2]IO_3$	$P2_1$	$[VO_4F_2]$, $[IO_3]$	9 × KDP	2.89	PM	[76]
$K_5(W_3O_9F_4)(IO_3)$	Pm	$[WO_5F]$, $[WO_4F_2]$, $[IO_3]$	11.0 × KDP	3.83	PM	[62]
$Sn(IO_3)_2F_2$	$P2_1$	$[SnO_4F_2]$, $[IO_3]$	3 × KDP	4.08	PM	[77]
$(NH_4)Bi_2(IO_3)_2F_5$	$P2_1$	$[BiO_2F_5]$, $[BiO_4F_4]$, $[IO_3]$	9.2 × KDP	3.88	PM	[64]
$BiIO_3F$	$C2$	$[BiO_4F_4]$, $[IO_3]$	11.5 × KDP	3.97	PM	[63]
$Bi_3OF_3(IO_3)_4$	$P6_3mc$	$[BiO_7F_2]$, $[IO_3]$	6.0 × KDP	3.70	PM	[78]
$Ce(IO_3)_2F_2{\cdot}H_2O$	$Ima2$	$[CeO_5F_4]$, $[IO_3]$	3 × KDP	2.6	PM	[79]
$Y(IO_3)_2F$	$P6_5$	$[YO_6F_2]$, $[IO_3]$	2 × KDP	3.91	PM	[80]
$CdIO_3F$	$P2_12_12_1$	$[CdO_5F_2]$, $[IO_3]$	6.2 × KDP	4.22	PM	[81]
$CsVO_2F(IO_3)$	$Pna2_1$	$[VO_5F]$, $[IO_3]$	1.1 × KTP	2.39	PM	[65]
$Pb_2GaF_2(SeO_3)_2Br$	$P2_1$	$[GaO_3F_3]$, $[SeO_3]$	4.5 × KDP	3.73	PM	[85]
$Pb_2GaF_2(SeO_3)_2Cl$	$P2_1$	$[GaO_3F_3]$, $[SeO_3]$	4.5 × KDP	4.32	PM	[67]
$Ba(MoO_2F)_2(TeO_3)_2$	$Aba2$	$[MoO_5F]$, $[TeO_3]$	7.8 × KDP	2.96	PM	[82]
$RbGa_3F_6(SeO_3)_2$	$P6_3mc$	$[GaO_2F_4]$, $[SeO_3]$	5.6 × KDP	3.57	PM	[85]
$Lu_3F(SeO_3)_4$	$P6_3$	$[LuO_7F]$, $[SeO_3]$	2.5 × KDP	3.57	PM	[86]
$K_2Bi_2(SeO_3)_3F_2$	Cm	$[BiO_6F_2]$, $[BiO_5F_2]$, $[SeO_3]$	15.0 × KDP	3.72	PM	[66]
$Bi_3(SeO_3)_3(Se_2O_5)F$	$P2_1$	$[BiO_6F]$, $[BiO_7]$, $[SeO_3]$	8 × KDP	3.80	PM	[83]
$Pb_2Cd(SeO_3)_2Br_2$	$P2_12_12_1$	$[CdO_6Br]$, $[PbO_xBr_y]$, $[SeO_3]$	1.8 × KDP	3.91	PM	[87]
$Pb_3(SeO_3)Br_4$	$P2_12_12_1$	$[PbBr_5O_2]$, $[PbBr_4O_3]$, $[SeO_3]$	1.0 × KDP	3.35	PM	[88]
$Sr_6Cd_2Sb_6O_7S_{10}$	Cm	$[SbOS_4]$, $[SbS_5]$, $[CdS_4]$	4.0 × AGS	1.89	PM	[46]
$Sr_5Ga_8O_3S_{14}$	$P2_12_12$	$[GaOS_3]$, $[GaO_4]$	0.8 × AGS	3.9	PM	[89]
Zn_3PI_3	$F\bar{4}3m$	$[ZnPI_3]$	2.7 × AGS	2.85	NPM	[69]
Zn_3AsI_3	$F\bar{4}3m$	$[ZnAsI_3]$	4.3 × AGS	2.38	NPM	[69]
Cd_3PI_3	$P6_3mc$	$[CdPI_3]$	3.5 × AGS	2.33	PM	[69]
Cd_3AsI_3	$P6_3mc$	$[CdAsI_3]$	5.1 × AGS	2.05	PM	[69]
$BaGeOSe_2$	$P2_12_12_1$	$[GeO_2Se_2]$	1.1 × AGS	3.20	PM	[44]
$SrZn_2S_2O$	$Pmn2_1$	$[ZnS_3O]$	2.0 × KDP	3.86	PM	[45]
$SrGeOSe_2$	$P2_12_12_1$	$[GeO_2Se_2]$	1.3 × AGS	3.16	PM	[92]
$Sr_3Ge_2O_4Se_3$	$R3m$	$[GeOSe_3]$	0.8 × AGS	2.96	PM	[93]

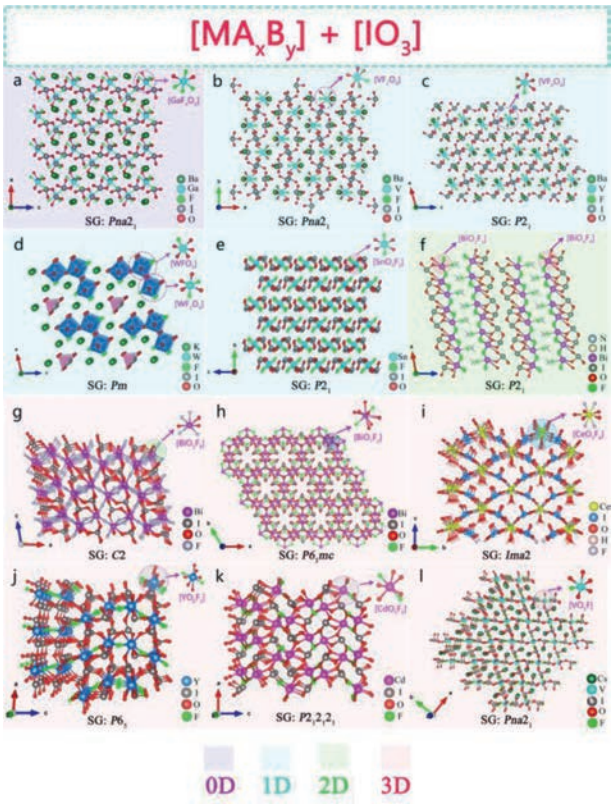

Fig. 1. Crystal structure of NLO materials with $[MA_xB_y]$ and $[IO_3]$ as NLO active units.

2.1.2. 1D chain formed by $[MA_xB_y]$ and $[IO_3]$ anionic groups

α,β-$Ba_2[VO_2F_2(IO_3)_2]IO_3$: Poeppelmeier *et al.* synthesized β-$Ba[VFO_2(IO_3)_2]$, α,β-$Ba_2[VO_2F_2(IO_3)_2]IO_3$ series [76] fluoroiodate compounds by hydrothermal method. β-$Ba[VFO_2(IO_3)_2]$ has a 0D isolated molecular structure which composed of $[VO_4F]$ mixed-anion polyhedra and two $[IO_3]$ units (Fig. 1c). α,β-Ba_2 $[VO_2F_2(IO_3)_2]IO_3$ polymorphs have similar crystal structure. Both of their crystal structures are composed of $[VO_4F_2]$ polyhedra and two $[IO_3]$ units to form a 1D chain, and Ba^{2+} are incorporated between the chains. However, in the α phase of polymorphic $Ba_2[VO_2F_2(IO_3)_2]IO_3$, the order of $[VO_4F]$ mixed-anion polyhedra and $[IO_3]$ units are better than that of β phase (Fig. 1b). Optical experiments show that they have a wide transparent region (~0.5–10.5 μm) in the IR band. Polymorphic $Ba_2[VO_2F_2(IO_3)_2]IO_3$ have type I phase matching ability, and can maintain a good balance between the wide E_g (> 2.5 eV) and strong SHG effect (~ 9 × KDP).

$K_5(W_3O_9F_4)(IO_3)$: Wu *et al.* obtained the colorless and transparent $K_5(W_3O_9F_4)(IO_3)$ crystal by hydrothermal method [62]. As shown in Fig. 1d, in the crystal structure of $K_5(W_3O_9F_4)(IO_3)$, $[WO_5F]$ and $[WO_4F_2]$ mixed-anion tetrahedrons form $[W_3O_{12}F_4]_\infty$ 1D chain through common vertex connection and $[IO_3]$ groups are isolated and scattered in the chain. Optical experiments show that the transparent region of $K_5(W_3O_9F_4)(IO_3)$ is 0.32–10.5 μm, and the indirect band gap is 3.83 eV. $K_5(W_3O_9F_4)(IO_3)$ had phase matching (PM) ability, and the SHG response was 11 × KDP and 0.5 × $AgGaS_2$ (AGS) (d_{36} = 23.6 ± 2.4 pm/V) under 1064 nm and 2100 nm laser irradiation, respectively. DFT calculations show that VBs maximum and CBs minimum of $K_5(W_3O_9F_4)(IO_3)$ are mainly determined by I 5p, W 5d, O 2p, and F 2p orbitals, which means that the optical properties of this compound are determined by mixed-anion group $[WO_3F]$ and single anion groups $[WO_4]$, $[IO_3]$.

$Sn(IO_3)_2F_2$: Luo *et al.* obtained a colorless and transparent fluorocompound iodate $Sn(IO_3)_2F_2$ by heating and cooling in a sealed

high-pressure reactor fitted with the gold liner [77]. As shown in Fig. 1e, the 1D chain structure of $Sn(IO_3)_2F_2$ is connected by two $[IO_3]$ groups and a low symmetry mixed-anion $[SnO_4F_2]$ polyhedral. Optical experiments show that $Sn(IO_3)_2F_2$ has a wide IR band transparent region and an E_g of 4.08 eV. In addition, the SHG powder test show that $Sn(IO_3)_2F_2$ exhibited type-I PM behavior, and the SHG response was 3 × KDP@1064 nm. DFT calculation shows that the introduction of highly polar halogen F based mixed-anion group in iodate is not only beneficial to SHG response, but also beneficial to increase the optical band gap.

2.1.3. 2D layered formed by [MA_xB_y] and [IO_3] anionic groups

$(NH_4)Bi_2(IO_3)_2F_5$ is representative compound of this type iodates. In 2019, Fan *et al.* prepared the first ammonium containing multianion fluoride iodate $(NH_4)Bi_2(IO_3)_2F_5$ by hydrothermal method with $KBi_2(IO_3)_2F_5$ as template [64]. As shown in the Fig. 1f, mixed-anion groups $[Bi(1)O_2F_5]$ and $[Bi(2)O_4F_4]$ form a 2D layered structure through co-edge connection and co-vertex connection with $[IO_3]$ group. It is worth noting that the NH_4^+ and F distributed between layers form N–H–F hydrogen bonds, which can strengthen the interaction between layers. Optical experimental results show that $(NH_4)Bi_2(IO_3)_2F_5$ has a wide E_g (3.88 eV) and a high transparency in the range of 2.5–6.8 μm. Kurtz powder test show that it had type-I PM ability, and SHG response was 9.2 × KDP@1064 nm. DFT calculations show that the VBs maximum and CBs minimum of $(NH_4)Bi_2(IO_3)_2F_5$ are mainly determined by the atomic orbitals of Bi, I, O and F atoms which indicates that optical properties of $(NH_4)Bi_2(IO_3)_2F_5$ are dominated by the $[Bi(1)O_2F_5]$, $[Bi(2)O_4F_4]$ and $[IO_3]$ groups.

2.1.4. 3D framework formed by [MA_xB_y] and [IO_3] anionic groups

$BiIO_3F$, $Bi_3OF_3(IO_3)_4$: Mao and Pan *et al.* designed and synthesized Bi-based fluorinated iodate $BiIO_3F$, $Bi_3OF_3(IO_3)_4$ by hydrothermal method [63,78]. As shown in Fig. 1g, the crystal structure of $BiIO_3F$ is built by $[BiO_4F_4]$ polyhedrons and interconnection of $[IO_3]$ groups to build a 3D framework structure. The network tunnel structure of $Bi_3OF_3(IO_3)_4$ is composed of $[BiO_7F_2]$ polyhedrons connected with $[IO_3]$ groups, and part of $[IO_3]$ groups are scattered in the tunnel holes (Fig. 1h). The experimental results show that $BiIO_3F$ and $Bi_3OF_3(IO_3)_4$ both have wide MIR transparent regions, with E_g of 3.97 eV and 3.70 eV, respectively. Kurtz powder test showed that they all had PM ability, and SHG strength was 11.5 and 6.0 × KDP@1064 nm, respectively.

$Ce(IO_3)_2F_2{\cdot}H_2O$: Abudouwufu *et al.* synthesized $Ce(IO_3)_2F_2{\cdot}H_2O$ by hydrothermal method [79]. As shown in Fig. 1i, its 3D framework structure formed by mixed-anionic $[CeO_5F_4]$ groups and $[IO_3]$ groups. In addition, two H atoms are connected with O atoms to form an H_2O unit interwoven with the tunnel holes. The experimental results show that the E_g of $Ce(IO_3)_2F_2{\cdot}H_2O$ is 2.6 eV, and SHG response is 3 × KDP@1064 nm with PM behavior. Theoretical analysis shows that VBs maximum of $Ce(IO_3)_2F_2{\cdot}H_2O$ is composed of I and O atomic orbitals, and the CBs minimum is composed of atomic orbitals of Ce. Therefore, its optical properties are mainly determined by the mixed-anionic $[CeO_5F_4]$ groups and $[IO_3]$ groups.

$Y(IO_3)_2F$, $Cd(IO_3)F$: Cao *et al.* synthesized rare earth fluorocompound iodate $Y(IO_3)_2F$ and transition metal fluorocompound iodate $Cd(IO_3)F$ by hydrothermal method [80,81]. As shown in the Fig. 1j, the crystal structure of $Y(IO_3)_2F$ is connected by complex coordinated group $[YO_6F_2]$ polyhedrons through co-edge to form a curved 1D chain, which is further connected by $[IO_3]$ group and finally forms a 3D skeleton structure. The 3D skeleton structure of $Cd(IO_3)F$ is composed of the mixed anion group $[CdO_5F_2]$ polyhedrons and $[IO_3]$ groups (Fig. 1k). Optical experiments show that $Y(IO_3)_2F$ and $Cd(IO_3)F$ have wide transparent region in the IR band, with E_g of 3.91 eV and 4.22 eV, respectively. Kurtz powder test show that they all had type I PM ability, and d_{ij} was 2 and 6.2 × KDP@1064 nm, respectively.

$CsVO_2F(IO_3)$: Chen *et al.* synthesized the mixed-anion fluoroiodate $C_SVO_2F(IO_3)$ by hydrothermal method [65]. $C_SVO_2F(IO_3)$ is the first alkali metal vanadifluoroioioate compound with 3D anion skeleton. It is formed by the interconnection of $[IO_3]$ and $[VO_5F]$ polyhedral groups (Fig. 1l). $C_SVO_2F(IO_3)$ has a wide MIR transparent region (0.5–10.5 μm) and E_g is 2.39 eV. Kurtz powder test show that it has type I PM behavior, and SHG response is 1.1 × KTP (d_{33} = 17.4 pm/V). DFT calculations show that the VBs maximum and the CBs minimum of $C_SVO_2F(IO_3)$ are mainly occupied by V, F and O atomic orbitals, which reveals that the optical properties of $C_SVO_2F(IO_3)$ are determined by the $[IO_3]$ and $[VO_5F]$ polyhedral groups.

2.2. [MA_xB_y] and [Se/TeO_3] as NLO active units

In addition to iodate, selenite and tellurite containing three coordinated $[SeO_3]$ and $[TeO_3]$ groups have also received more and more attention in the nonlinear optics field [67]. Similar to $[IO_3]$ groups, the combination of planar π-conjugated groups $[SeO_3]$ and $[TeO_3]$ with complex coordinated groups $[MA_xB_y]$ favors to the generation of IR NLO crystals with excellent comprehensive performance. Recently, Mao, Ye, OK and other research groups have found a series of IR NLO materials of this type, such as $Ba(MoO_2F)_2(QO_3)_2$(Q = Se, Te) [82], $K_2Bi_2(SeO_3)_3F_2$ [66], $Bi_3(SeO_3)_3(Se_2O_5)F$ [83]. In this part, based on the anionic crystal structure dimension from 1D to 3D, this type of NLO crystals were comprehensively summarized from the perspective of structure-property relationship.

2.2.1. 1D chain formed by [MA_xB_y] and [SeO_3] anionic groups

Lin and You *et al.* synthesized isomorphically $Pb_2GaF_2(SeO_3)_2X$ (X = Cl, Br) by hydrothermal method [67,84]. They have similar crystal structure. Taking $Pb_2GaF_2(SeO_3)_2Cl$ as an example, its crystal structure is connected by $[GaO_3F_3]$ polyhedron and $[SeO_3]$ group to form a 1D chain structure, and each Cl atom connects two Pb atoms along the *ab* direction (Fig. 2a). The results of optical experiment show that both of them have wide MIR transparent region, and the E_g are 4.32 eV and 3.73 eV for $Pb_2GaF_2(SeO_3)_2Cl$ and $Pb_2GaF_2(SeO_3)_2Br$, respectively. Under 1064 nm laser irradiation, their SHG response is 4.5 × KDP, and they have type I PM capability. Theoretical analysis shows that $[GaO_3F_3]$ and $[SeO_3]$ units play a major role in their large d_{ij}.

2.2.2. 2D layered formed by [MA_xB_y] and [Se/TeO_3] anionic groups

$Ba(MoO_2F)_2(QO_3)_2$ (Q = Se, Te): Liang *et al.* synthesized the colorless and transparent alkaline earth metal fluoroselenite and fluorotellurite compounds $Ba(MoO_2F)_2(QO_3)_2$ (Q = Se, Te) by hydrothermal method [82]. They belong to NCS orthogonal space group *Aba*2 (No. 41). They have similar crystal structures. Taking $Ba(MoO_2F)_2(SeO_3)_2$ as an example, there are two NAUs of mixed anion $[MoO_5F]$ and $[SeO_3]$ in the structure. They form a 2D layer by sharing vertexs, and Ba^{2+} is scattered between the layers (Fig. 2b). It is worth noting that the SHG intensity (7.8 × KDP@1064 nm) of $Ba(MoO_2F)_2(TeO_3)_2$ with PM ability is significantly greater than that of $Ba(MoO_2F)_2(SeO_3)_2$ (2.8 × KDP@1064 nm). This indicates that the SHG activity of $[TeO_3]$ group is stronger than that of $[SeO_3]$ group. Their E_g are 2.96 eV and 3.23 eV, respectively. DFT calculations show that the VBs maximum of $Ba(MoO_2F)_2(TeO_3)_2$ is mainly occupied by atomic orbitals of O 2p and F 2p, while CBs minimum is mainly occupied by atomic orbitals of O 2p, Te 5p and Mo 4d, which indicates that its optical properties are mainly determined by $[MoO_5F]$ and $[TeO_3]$ groups.

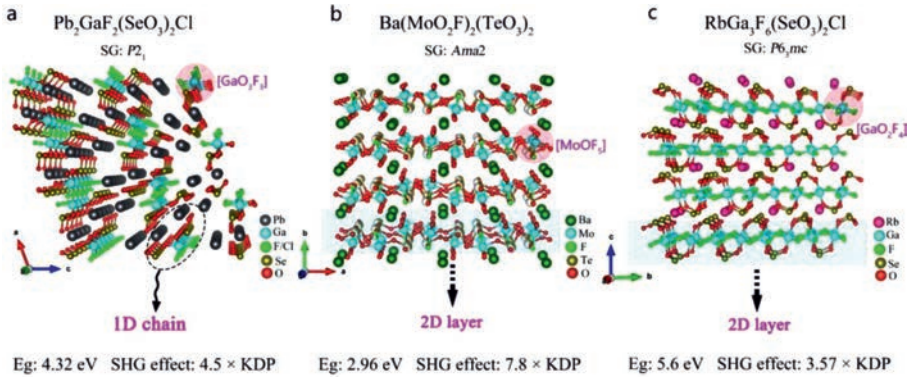

Fig. 2. Crystal structure and NLO performance of (a) $Pb_2GaF_2(SeO_3)_2Cl$, (b) $Ba(MoO_2F)_2(TeO_3)_2$ and (c) $RbGa_3F_6(SeO_3)_2$.

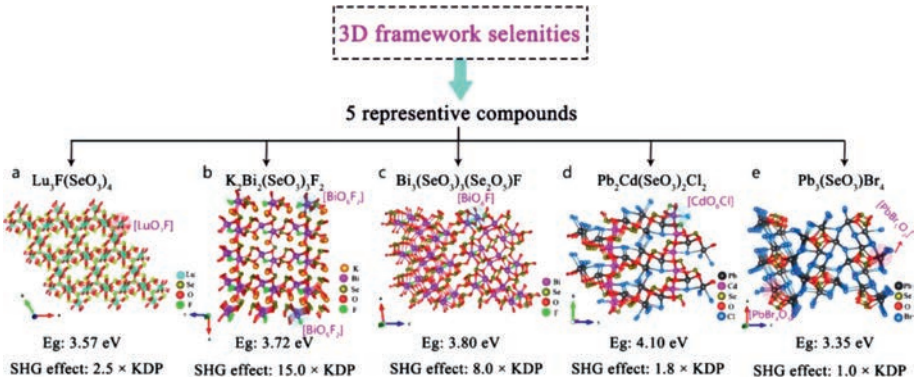

Fig. 3. Crystal structure and NLO performance of 5 representative 3D framework selenities.

$RbGa_3F_6(SeO_3)_2$: Wu *et al.* designed and synthesized the alkali metal fluoride selenite compounds $RbGa_3F_6(SeO_3)_2$ by hydrothermal method [85]. In the crystal structure of $RbGa_3F_6(SeO_3)_2$, $[SeO_3]$ groups connect the mixed-anion groups $[GaO_2F_4]$ (Fig. 2c). Optical experiments show that $RbGa_3F_6(SeO_3)_2$ have a wide transparent region in IR wavelengths. Kurtz powder test showed that $RbGa_3F_6(SeO_3)_2$ have type I phase matching ability, and SHG strength was 5.6 × KDP@1064 nm and E_g is 3.57 eV. According to the calculated PDOS diagram, the VBs maximum and CBs minimum are mainly occupied by the atomic orbitals of Ga, F, Se and O atoms, which indicates that the optical properties of $RbGa_3F_6(SeO_3)_2$ are mainly determined by the $[SeO_3]$ and $[GaO_2F_4]$ units.

2.2.3. 3D framework formed by $[MA_xB_y]$ and $[SeO_3]$ anionic groups

$Lu_3F(SeO_3)_4$: Wu *et al.* synthesized the colorless and transparent rare earth metal fluoroselenite compound $Lu_3F(SeO_3)_4$ by hydrothermal method [86]. The 3D frame structure of $Lu_3F(SeO_3)_4$ is formed by twisted $[LuO_7F]$ polyhedron and planar p-conjugated $[SeO_3]$ groups (Fig. 3a). $Lu_3F(SeO_3)_4$ has a wide transparent region in IR wavelengths and E_g is 3.57 eV. Kurtz powder test show that $Lu_3F(SeO_3)_4$ exhibits PM behavior, and the SHG strength of $Lu_3F(SeO_3)_4$ is 2.5 × KDP@1064 nm. DFT calculation revealed that the optical properties of $Lu_3F(SeO_3)_4$ are mainly determined by $[LuO_7F]$ and $[SeO_3]$ groups.

$K_2Bi_2(SeO_3)_3F_2$, $Bi_3(SeO_3)_3(Se_2O_5)F$: Shi *et al.* synthesized a colorless and transparent Bi-based alkali metal selenite $K_2Bi_2(SeO_3)_3F_2$ by hydrothermal method [66]. In the crystal structure of $K_2Bi_2(SeO_3)_3F_2$, Bi(1) atoms connect six O atoms and two F atoms to form a $[BiO_6F_2]$ group, and Bi(2) atoms link to five O atoms and two F atoms to form $[BiO_5F_2]$ group. $[BiO_6F_2]$ group and $[BiO_5F_2]$ group share one O and one F atom to form a 1D chain structure, and $[IO_3]$ connects these 1D chains to finally form a 3D framework structure (Fig. 3b). The transparent region of the growing block $K_2Bi_2(SeO_3)_3F_2$ crystal covers the important band 3–5 μm in the IR region. $K_2Bi_2(SeO_3)_3F_2$ with phase matching ability can maintain a balance between the wide E_g (3.72 eV) and the strong SHG response (15 × KDP @1064 nm). DFT calculation indicated that the optical properties are mainly determined by $[BiO_xF_y]$ and $[SeO_3]$ groups.

Chung *et al.* synthesized colorless and transparent Bi-based selenite fluoride $Bi_3(SeO_3)_3(Se_2O_5)F$ by hydrothermal method [83]. There are three active NLO groups $[BiO_7]$, $[BiO_6F]$ and $[SeO_3]$ in the crystal structure, in which $[BiO_7]$ and $[BiO_6F]$ polyhedra form a 2D layer through co-edge connection, and $[SeO_3]$ further connects the 2D layer to form a 3D frame structure (Fig. 3c). The optical results show that $Bi_3(SeO_3)_3(Se_2O_5)F$ has a wide IR transparent window. Furthermore, $Bi_3(SeO_3)_3(Se_2O_5)F$ exhibits wide band gap (3.80 eV) and strong SHG response (8.0 × KDP@1064 nm) with type-I PM behavior. Theoretical analysis shows that the strongly twisted mixed-anion $[BiO_6F]$ polyhedron play an important role in its good comprehensive performance.

$Pb_2Cd(SeO_3)_2Cl_2$, $Pb_3(SeO_3)Br_4$: Chen and Ma *et al.* synthesized lead halogen selenite $Pb_2Cd(SeO_3)_2Cl_2$ and $Pb_3(SeO_3)Br_4$ by hydrothermal method [87,88]. As shown in Fig. 3d, the crystal structure of $Pb_2Cd(SeO_3)_2Cl_2$ is composed of $[CdO_6Br]$, $[PbO_xBr_y]$ and $[SeO_3]$ groups. They interpenetrate and connect to form a 3D framework structure. The crystal structure of $Pb_3(SeO_3)Br_4$ has three kinds of NAUs, *e.g.*, $[PbBr_5O_2]$, $[PbBr_4O_3]$ and $[SeO_3]$, in which $[PbBr_5O_2]$ and $[PbBr_4O_3]$ form 3D tunnel structure by sharing Br atoms (Fig. 3e). Under 1064 nm laser irradiation, $Pb_2Cd(SeO_3)_2Cl_2$ and $Pb_3(SeO_3)Br_4$ with type I phase matching ability exhibit 1.8 and 1.0 times SHG effects that of KDP, respectively. Their E_g are 4.10 eV for $Pb_2Cd(SeO_3)_2Cl_2$ and 3.35 eV for $Pb_3(SeO_3)Br_4$, respectively. DFT calculations suggest the VBs maximum and CBs minimum of $Pb_2Cd(SeO_3)_2Cl_2$ mainly occupy by Pb, Se, Cl, O atomic

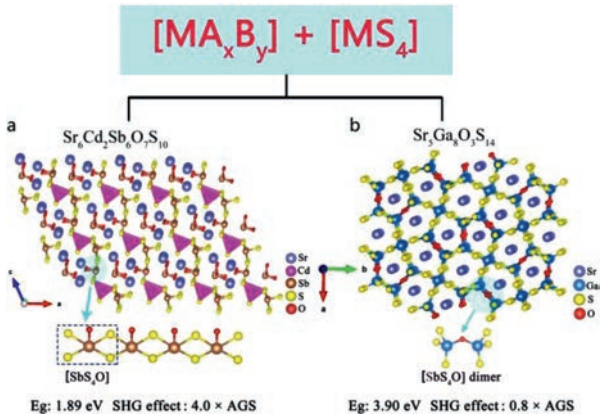

Fig. 4. Crystal structure and NLO performance of $Sr_6Cd_2Sb_6O_7S_{10}$ and $Sr_5Ga_8O_3S_{14}$.

orbitals, which suggests that its optical properties are mainly depends on $[PbO_xBr_y]$ and $[SeO_3]$ groups. The VBs maximum and CBs minimum of $Pb_3(SeO_3)Br_4$ mainly occupy by the orbitals all constituent atoms, suggesting that its optical properties are mainly determinated by $[PbBr_5O_2]$, $[PbBr_4O_3]$ and $[SeO_3]$ groups.

In summary, most of the IR NLO crystals composed of the complex coordinated group $[MA_xB_y]$ and tri-coordinated group $[Se/TeO_3]$ have a 3D framework structure. Similar to iodates, they all have good optical anisotropy and all have phase matching capabilities. According to theoretical analysis, the introduction of highly electronegative halogens, such as F, Cl, Br, is in favor of enhancing the E_g of iodate. Most compounds with complex coordinated groups $[MA_xB_y]$ and $[Se/TeO_3]$ SBUs have ideal optical band gaps (larger than 3.5 eV). It is worth noting that the compounds with $[BiO_xF_y]$ and $[SeO_3]$ as SBUs have good overall performance (good phase matching ability, large optical band gap, strong SHG effect).

2.3. $[MA_xB_y]$ and $[MS_4]$ as NLO active units

Compared with oxygen-based tri-coordinated groups, few IR NLO compounds are composed of mixed anions $[MA_xB_y]$ and $[MS_4]$ as SBUs. Recently, Wang *et al.* designed and synthesized two compounds $Sr_6Cd_2Sb_6O_7S_{10}$ [46] and $Sr_5Ga_8O_3S_{14}$ [89] by combining the complex coordinated group $[MO_xS_y]$ with the tetra-coordinated group $[MS_4]$. Herein, these two compounds are selected as representatives to discuss the influence of SBUs functional groups on optical properties of this type compound.

$Sr_6Cd_2Sb_6O_7S_{10}$: Wang *et al.* obtained the red $Sr_6Cd_2Sb_6O_7S_{10}$ crystal by solid-phase synthesis [46]. As shown in Fig. 4a, its 2D layered structure is formed by the mixed-anion SBUs $[SbOS_4]$, the single anion poly-coordinated group $[SbS_5]$ and the tetra-coordinated group $[CdS_4]$ connected to each other on the *bc* plane. The powder frequency doubling test shows that $Sr_6Cd_2Sb_6O_7S_{10}$ has phase matching ability. When the particle size is 150–210 μm, the SHG effect is 4.0 × AGS in 2090 nm. The bandgap of $Sr_6Cd_2Sb_6O_7S_{10}$ is 1.89 eV. Atomistic first principles calculations show that the $5S^{2-}$ electron $[SbO_xS_{5-x}]^{7-}$ (x = 0, 1) groups make a major contribution to its strong SHG effect. In addition, further theoretical analysis shows that the mixed-anionic group $[SbOS_4]$ has a greater contribution to the d_{ij} than the single-anionic unit $[SbS_5]$.

$Sr_5Ga_8O_3S_{14}$: Wang *et al.* obtained colorless and transparent melilite-derived oxysulfide $Sr_5Ga_8O_3S_{14}$ crystals by solid-phase synthesis [89]. As shown in Fig. 4b, the crystal structure consists of a mixed polyanion group $[GaOS_3]$ tetrahedron and $[GaS_4]$ tetrahedron group connected to form a 3D framework structure, with Sr^{2+} scattered in the tunnel holes. Optical research shows that $Sr_5Ga_8O_3S_{14}$ with NPM behavior exhibits a large E_g (3.9 eV) and a strong SHG effect (0.8 × AGS @2090 nm). It has a wide IR transparent area of 0.3–13.4 μm. Theoretical calculations show that the mixed polyanionic group $[GaOS_3]$ tetrahedron and $[GaS_4]$ tetrahedron group play the main contribution to the SHG effect of $Sr_5Ga_8O_3S_{14}$.

To sum up, the reasonable combination of complex coordinated groups $[MA_xB_y]$ and other single anionic groups, such as $[IO_3]$, $[SeO_3]$, $[TeO_3]$, $[MS_4]$, is a very effective strategy to design and synthesize great-performance IR NLO crystals. At present, this type of NLO material, complex coordinated groups $[MA_xB_y]$ and tri-coordinated groups $[IO_3]$, $[SeO_3]$, $[TeO_3]$ as building units, has been widely explored. They all have good phase matching capabilities, and most of them have a wide optical band gap. The key issue is how to effectively improve the NLO effect. Interestingly, $[MO_xF_y]$ (M = V, Mo, W, Bi, *etc.*) composed of mixed anion groups centered on transition metal or metal with lone pair electrons not only provide strong SHG contribution, but also help guide tri-coordinated groups $[IO_3]$, $[SeO_3]$, $[TeO_3]$ to arrange orderly. Therefore, most compounds with this group have excellent comprehensive properties, such as $K_5(W_3O_9F_4)(IO_3)$, $BiIO_3F$, $Ba_2[VO_2F_2(IO_3)_2]IO_3$, $(NH_4)Bi_2(IO_3)_2F_5$, $CsVO_2F(IO_3)$, $Ba(MoO_2F)_2(TeO_3)_2$, $K_2Bi_2(SeO_3)_3F_2$ and $Bi_3(SeO_3)_3(Se_2O_5)F$. All of compounds above can keep a good balance between strong SHG reponse with phase matching ability and wide E_g. The combination of complex coordinated group $[MA_xB_y]$ and tetra-coordinated group $[MS_4]$ has the potential to design NLO crystals with strong SHG effect. For example, $Sr_6Cd_2Sb_6O_7S_{10}$ has an extremely strong SHG intensity of 4 times that of AGS.

2.4. Halides-based pnictides

Chen *et al.* solved the shortcomings of the band gap of phosphorus compounds by introducing strong electronegative heavy halogen "I" into phosphorus compounds [69]. They obtain four kinds of iodinated phosphorus NLO crystals by heterovalent anion substitution strategy, namely $M^{II}_3PnI_3$ (M^{II} = Zn, Cd; Pn = P, As). It has a defective diamond-like structure, and the mixed anion $[M^{II}PnI_3]$ tetrahedral groups arrange toward the same direction. Taking $ZnPI_3$ as an example, as shown in Fig. 5a, its structure stacked by $[ZnPI_3]$ tetrahedrons along [111] direction by sharing vertexes. The optical experiment results show that their E_g are 2.85 eV and 2.38 eV, respectively. Their SHG effect are 2.7 and 4.3 × AGS, respectively, without PM capability. Taking $CdPI_3$ as an example, as shown in figure, its structure stacked by $[CdPI_3]$ tetrahedrons along [001] direction by sharing vertexes (Fig. 5b). The optical experiment results show that their E_g are 2.44 eV and 2.05 eV, respectively. Their SHG effect are 2.7 and 4.3 × AGS, respectively, with type-I PM behavior.

2.5. Oxychalcogenides

Compared with traditional oxides and chalcogenides, oxychalcogenides have received few attentions in NLO region. In recent years, oxychalcogenides has attracted people's attention. Different research groups have designed and synthesized several IR NLO crystals with mixed anions $[MO_xQ_y]$ (Q = S, Se) as SBUs [90–92]. Herein, the crystal structure and optical properties of this type compounds are analyzed in details.

$AEGeOSe_2$ (AE = Ba, Sr): Liu *et al.* synthesized oxychalcogenides $BaGeOSe_2$ and $SrGeOSe_2$ by solid-phase method [44,45]. They have similar crystal structures. As shown in Fig. 6a, their crystal structures are composed of mixed-anion groups $[GeO_2Se_2]$ connected by common edges to form a 1D chain structure, with Ba^{2+} and Sr^{2+} scattered among the chains. The optical band gap of $BaGeOSe_2$ and $SrGeOSe_2$ are 3.20 eV and 3.14 eV, respectively. Under 1400 and 2050 nm laser irradiation, both of them exhibit

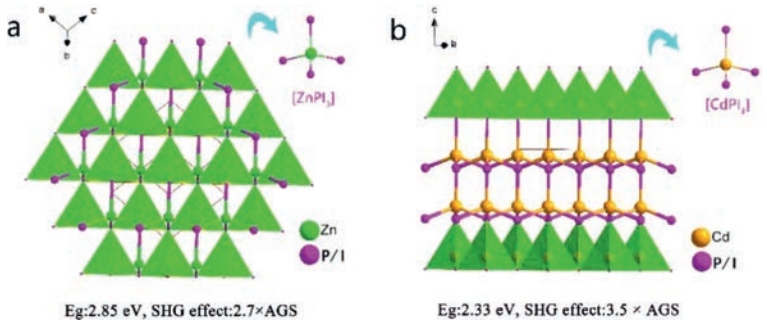

Fig. 5. Crystal structure of $ZnPI_3$ and $CdPI_3$.

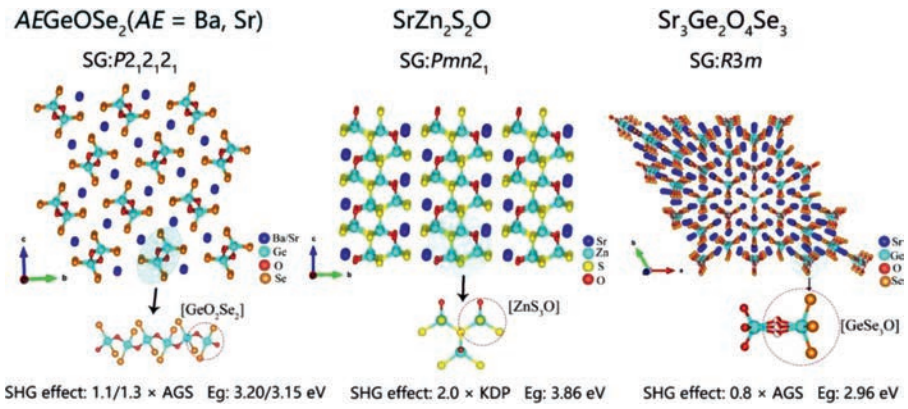

Fig. 6. Crystal structure and NLO performance of (a) $AEGeOSe_2$(AE = Ba, Sr), (b) $SrZn_2S_2O$ and (c) $Sr_3Ge_2O_4Se_3$.

type-I PM behavior and SHG signal output intensity are 1.1 and 1.3 times that of benchmark AGS. Theoretical analysis shows that complex coordinated groups [GeO_2Se_2] make major contributions to their strong SHG effect.

$SrZn_2S_2O$: Loye *et al.* obtained NCS polar oxysulfide $SrZn_2S_2O$ by solid-phase synthesis. As shown in Fig. 6b, its 2D layered structure consists of complex coordinated tetrahedral groups [ZnS_3O] connected to each other along the *ac* plane. The powder frequency doubling absorption spectrum curve shows that $SrZn_2S_2O$ has a large E_g of 3.86 eV. DFT calculations show that the VBs maximum of $SrZn_2S_2O$ is mainly occupied by atomic orbitals of O 2p and S 3p, while the CBs minimum are mainly occupied by atomic orbitals of Zn 4s and Zn 4p, which indicates that its optical properties are mainly determined by mixed-anion [ZnS_3O] groups.

$Sr_3Ge_2O_4Se_3$: Xing *et al.* obtained colorless and transparent $Sr_3Ge_2O_4Se_3$ crystals through solid-phase synthesis [93]. As shown in Fig. 6c, the crystal structure of $Sr_3Ge_2O_4Se_3$ contains [$GeOSe_3$] mixed anion group and [GeO_4] tetra-coordinated group, which are connected to form a unique dumbbell-like dimer $[Ge_2O_4Se_3]^{6-}$. The energy band gap of $Sr_3Ge_2O_4Se_3$ is 2.96 eV. Under 1064 nm laser irradiation, $Sr_3Ge_2O_4Se_3$ exhibits phase matching behavior, and the NLO response is 0.8 times that of AGS. DFT calculation indicates that the VBs maximum of $Sr_3Ge_2O_4Se_3$ are mainly determined by the atomic orbits of O 2p and Se 4s, and the CBs minimum are predominantly composed of Ge 4s and 4p orbits. It is worth noting that the mixed anion group [$GeOSe_3$] 's contribution to SHG effect is significantly stronger than that of the single anionic group [GeO_4].

In conclusion, the comprehensive performance of IR NLO crystals with complex coordinated groups as SBUs exhibit superior performance to that of traditional single-anionic compounds. In comparison to traditional phosphides, $M^{II}_3PnI_3$ halides-based pnictides inherit the large effect of phosphides, and also have an increased optical band gap. The oxychalcogenides series also exhibit superior optical properties to conventional oxides and chalcogenides.

3. UV/DUV complex coordinated NLO materials

In the field of UV and DUV nonlinear optics, common single-anion NAUs are composed of oxygen-based tri-coordinated groups and tetra-coordinated groups, *e.g.*, [BO_3], [NO_3], [CO_3], [PO_4], [SO_4] [20,90–96]. In the last few years, a large number of UV/DUV NLO crystals with good performance have been designed and synthesized by different research groups in combination of the above groups with the mixed anion groups [MA_xB_y]. Pan, Ye, Halasyamani and other teams applied KBBF as a template to design and synthesize many DUV NLO crystals with excellent performance. Many of these compounds not only have better comprehensive properties than KBBF, but also are expected to overcome the limitations of the layered growth habit. In addition, Mao, Ye, Zou and Halasyamani have synthesized a series of novel UV and DUV NLO materials by combining tri-coordinated ([NO_3], [CO_3]) and tetra-coordinated groups ([PO_4], [SO_4]) with mixed-anion group [MO_xF_y]. According to the types and structural characteristics of the anions, the crystals can be divided into: (1) KBBF-derived crystals; (2) nitrate and carbonate; (3) phosphates; (4) sulfate. This part specifically summarizes UV/DUV complex coordinated NLO materials in recent five years on the relationship between crystal structure and optical properties (Table 2) in combination to theoretical analysis results.

3.1. KBBF-derived crystals

KBBF has been regarded as the benchmark in this field as one of the most commercialized DUV NLO materials [47,48]. The discussion on the structure-property analysis of KBBF crystals has been reported in other literatures will not be summarized here. This

Table 2
Optical properties of UV/DUV complex coordinated NLO crystals.

Compounds	SG	SBUs	SHG effect	Cutoff edge	PM/NPM	Type I PM SHG limit	Ref.
CsB_4O_6F	$Pna2_1$	[BO_3], [BO_3F]	1.9 × KDP	155 nm	PM	175 nm	[32]
RbB_4O_6F	$Pna2_1$	[BO_3], [BO_3F]	0.8 × KDP	< 200 nm	PM	165 nm	[49]
$CsKB_8O_{12}F_2$	$P32_1$	[BO_3], [BO_3F]	1.9 × KDP	< 200 nm	PM	170 nm	[49]
NaB_4O_6F	$C2$	[BO_3], [BO_3F]	0.9 × KDP	< 180 nm	PM	< 166 nm	[50]
$Ba_3Mg_3(BO_3)_3F_3$	$Pna2_1$	[BO_3], [MgO_4F_2]	1.8 × KDP	184 nm	PM	310 nm	[51]
$CaB_5O_7F_3$	$Cmc2_1$	[BO_3], [BO_3F]	2.0 × KDP	< 180 nm	PM	183 nm	[54]
$CsAlB_3O_6F$	$Pna2_1$	[BO_3], [AlO_3F]	2.0 × KDP	< 190 nm	PM	182 nm	[96]
$LaB_4O_6(OH)_2Cl$	Cc	[BO_3], [$BO_3(OH)$]	2.3 × KDP	< 180 nm	PM	–	[97]
$NH_4B_4O_6F$	$Pna2_1$	[BO_3], [BO_3F]	1.2 × KDP	156 nm	PM	158 nm	[50]
$NH_4Be_2BO_3F_2$	$R32$	[BO_3], [BeO_3F]	1.2 × KDP	153 nm	PM	173.9 nm	[57]
γ-Be_2BO_3F	$R32$	[BO_3], [BeO_3F]	2.3 × KDP	< 190 nm	PM	146 nm	[57]
Pb_2BO_3I	$P321$	[BO_3], [PbO_3I_2]	10.0 × KDP	330 nm	PM	–	[98]
$PbB_5O_7F_3$	$Cmc2_1$	[BO_3], [BO_3F]	6.0 × KDP	< 225 nm	PM	–	[53]
$SrB_5O_7F_3$	$Cmc2_1$	[BO_3], [BO_3F]	1.6 × KDP	< 180 nm	PM	~ 180 nm	[52]
$C(NH_2)_3SO_3F$	$R3m$	[SO_3], [SO_3F]	5.0 × KDP	200 nm	PM	< 200 nm	[77]
$Pb_2(NO_3)_2(H_2O)F_2$	$Amm2$	[NO_3], [PbO_9F_2]	12 × KDP	300 nm	PM	–	[99]
$KMgCO_3F$	$P\bar{6}2m$	[CO_3], [MgO_3F_2]	3.0 × KDP	< 200 nm	PM	–	[101]
$NaZnCO_3F$	$P\bar{6}2m$	[CO_3], [ZnO_3F_2]	2.75 × KDP	230 nm	PM	–	[102]
$Ba_2NaClP_2O_7$	$P4bm$	[PO_4], [NaO_4Cl_2]	0.9 × KDP	< 176 nm	PM	–	[59]
$BaZn(PO_4)F$	$Pna2_1$	[PO_4], [ZnO_4F]	0.26 × KDP	< 190 nm	PM	–	[103]
$CsSiP_2O_7F$	$P2_1$	[PO_4], [SiO_5F]	0.7 × KDP	< 190 nm	PM	–	[60]
$K_2Sb(P_2O_7)F$	$P4bm$	[PO_4], [SbO_4F]	4.0 × KDP	216 nm	PM	–	[105]
$Na_3Sc_2(PO_4)_2F_3$	$I4mm$	[PO_4], [ScO_4F_2]	0.26 × KDP	255 nm	PM	–	[106]
$CsSbF_2SO_4$	$Pna2_1$	[SO_4], [SbO_2F_2]	3.0 × KDP	240 nm	PM	–	[107]
$RbSbSO_4Cl_2$	$P2_12_12_1$	[SO_4], [SbO_3Cl_2]	2.7 × KDP	347 nm	PM	–	[109]
$NH_4SbF_2SO_4$	$Pna2_1$	[SO_4], [SbO_2F_2]	0.7 × KDP	266 nm	PM	–	[108]
$Sn[B_2O_3F_2]$	$P31m$	[BO_3F]	> 1.0 × KDP	243 nm	PM	–	[110]
$NaNH_4PO_3F{\cdot}H_2O$	Pc	[PO_3F]	1.1 × KDP	< 176 nm	PM	194 nm	[69]
$BaF_2TeF_2(OH)_2$	$Pmn2_1$	[TeO_2F_2]	3.0 × KDP	205 nm	PM	–	[61]

part focuses on the analysis of a series of new DUV NLO materials derived from KBBF template and taking representative compounds as an example. Figs. 7–10 show their crystal structure. Performance enhancement method originated from ntrinsic property is analyzed by relationship between their crystal structure and optical properties of KBBF. Depending on the type of compound, it is divided into six sections according to the type of compounds.

3.1.1. AB_4O_6F (A = Rb, Cs, K, Na, NH_4) family

Wang and their team designed and synthesized a series of colorless and transparent KBBF-derived fluorooxoborate, including CsB_4O_6F, RbB_4O_6F, $CsKB_8O_{12}F_2$, NaB_4O_6F, $NH_4B_4O_6F$ [32,49–51]. These crystals were prepared by solid phase reaction method. $CsKB_8O_{12}F_2$ and NaB_4O_6F belong to NCS space groups $P32_1$ and $C2$, respectively. The crystal structure of these compounds is similar to KBBF, in which the cation K^+ is replaced by Cs^+, Rb^+, Cs^+ and K^+ mixed cations, Na^+ and NH_4^+, respectively. As shown in Fig. 7, the interlayer spacing of CsB_4O_6F, $CsKB_8O_{12}F_2$ and $NH_4B_4O_6F$ is significantly smaller than that of KBBF (6.25 Å), indicating that their interlayer forces are stronger than KBBF's. In addition, the substitution of [BO_3F] for [BeO_3F] can eliminate the toxicity of Be element. Optical experiments show that they all have a wide transparent region in the UV/DUV band, and these compounds have short ultraviolet cut-off edge: CsB_4O_6F (155 nm), RbB_4O_6F (< 200 nm), $CsKB_8O_{12}F_2$ (< 200 nm), NaB_4O_6F (< 180 nm), $NH_4B_4O_6F$ (156 nm). In addition, all of these compounds have phase matching capability. As shown in Table 2, the SHG effect of CsB_4O_6F, $CsKB_8O_{12}F_2$ and $NH_4B_4O_6F$ is stronger than that of KBBF (1.2 × KDP@1064 nm) under the irradiation of 1064 nm laser. More importantly, the theoretical analysis shows that their shortest second harmonic phasematching wavelength are less than 200 nm. All these properties indicate that these crystals are promising to be the next generation DUV materials. DFT calculation shows that the optical properties of AB_4O_6F (A = Rb, Cs, K, Na, NH_4) family are mainly determined by the anion layer $[B_4O_6F]^-{}_\infty$.

3.1.2. $M(B_5O_7)F_3$ (M = Sr, Ca, Pb)

Pan's team designed and synthesized KBBF-type $SrB_5O_7F_3$ and $CaB_5O_7F_3$ crystals [52,54]. $SrB_5O_7F_3$ and $CaB_5O_7F_3$ have a 2D layered structure. The structural units [$B_5O_7F_3$] are composed of three [BO_3F] units and two [BO_3] units. These [$B_5O_7F_3$] units form 2D layer in the *ac* plane by co-apex connection (Fig. 8a). The NLO response of $SrB_5O_7F_3$ and $CaB_5O_7F_3$ are 1.6 and 2.0 × KDP@ 1064 nm, respectively. Their ultraviolet cut-off edges are less than 180 nm. In addition, theoretical calculations show that their shortest second harmonic phasematching wavelengths are 180 nm and 183 nm, respectively. All these properties indicate that $SrB_5O_7F_3$ and $CaB_5O_7F_3$ have the potential to be the next generation DUV materials. According to DFT calculation, the VBs maximum of $CaB_5O_7F_3$ is mainly determined by O 2p and F 2p atomic orbitals, while CBs minimum is mainly determined by Ca 3p and B 2p atomic orbitals. Therefore, the optical properties of $CaB_5O_7F_3$ are determined by the Ca^{2+} and [$B_5O_7F_3$] units. This is different from AB_4O_6F (A = Rb, Cs, K, Na, NH_4) family compounds.

Pan *et al.* designed and synthesized a Pb-based $PbB_5O_7F_3$ crystal that is isomorphic to $SrB_5O_7F_3$ [53]. Its anionic layered framework is similar to $SrB_5O_7F_3$, and stereochemically active lone-pair (SCALP) cations are connected by Pb-F bonds to form a 3D framework structure (Fig. 8b). The distance between adjacent layers (4.38 Å) is significantly smaller than that of KBBF (6.25 Å). $PbB_5O_7F_3$ has a strong SHG effect (6.0 × KDP@1064 nm), showing a PM capability. In addition, the ultraviolet cut-off edge of $PbB_5O_7F_3$ is less than 225 nm, which is significantly less than other Pb-based NLO compounds. According to theoretical calculations, the VBs maximum of $PbB_5O_7F_3$ are predominately determined by O 2p, F 2p, B 2p and Pb 6s, p orbitals. The CBs minimum is mainly determined by O 2p, B 2p, Pb 6s, p atomic orbitals. Obviously, due to the influence of Pb, the band gap of $PbB_5O_7F_3$ is smaller than that of Sr-based compounds. Further theoretical analysis shows that due to the high electronegativity of F and the O-B-F bands, the band gap of $PbB_5O_7F_3$ is larger than other Pb-containing compounds. The SHG-density method proves that the

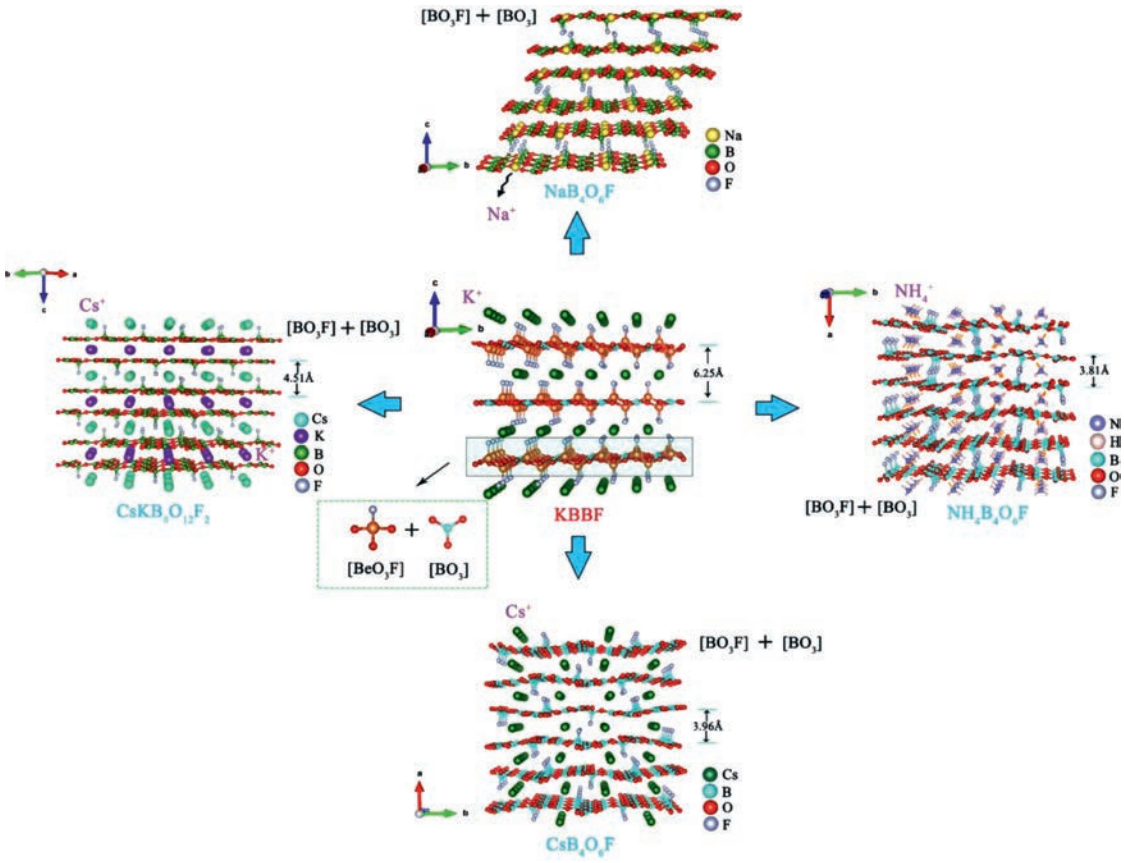

Fig. 7. Crystal structure of AB_4O_6F (A = Rb, Cs, K, Na, NH_4) series compounds.

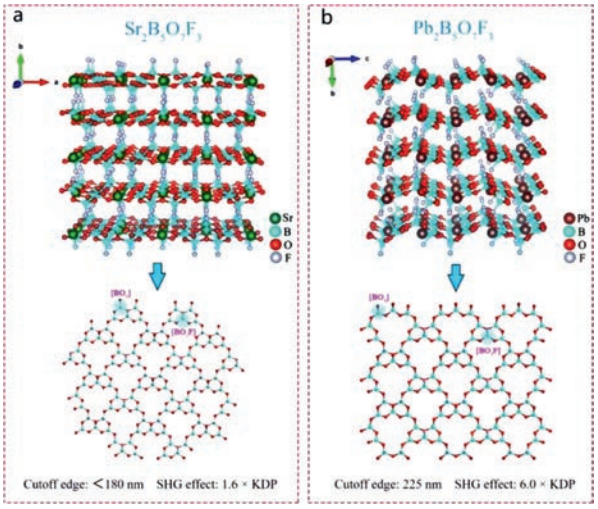

Fig. 8. Crystal structure and NLO performance of $SrB_5O_7F_3$ and $PbB_5O_7F_3$.

strong SHG response of $PbB_5O_7F_3$ is mainly derived from the co-operation of $[BO_3]$, $[BO_3F]$, $[PbO_6F_3]$ groups.

3.1.3. $Ba_3Mg_3(BO_3)_3F_3$, $CsAlB_3O_6F$

Mutailipu *et al.* designed and synthesized polymorphs $Ba_3Mg_3(BO_3)_3F_3$ by solid-phase synthesis method using SBBO as a template [55]. α- and β-$Ba_3Mg_3(BO_3)_3F_3$ have similar 2D layered structure. Their crystal structures are connected by $[BO_3]$ groups and $[MgO_4F_2]$ polyhedrons to form 2D layers in *bc* and *ab* planes, respectively, and further connected by Mg-F bond to form 3D framework structure (Fig. 9a). It is worth noting that α-$Ba_3Mg_3(BO_3)_3F_3$ has grown high-quality large-size ($16 \times 14 \times 8$ mm^3) crystals. Optical experiment tests show that phasematching α-$Ba_3Mg_3(BO_3)_3F_3$ has a strong SHG response ($1.8 \times$ KDP@1064 nm) and a short ultraviolet cut-off edge (184 nm). All these properties indicate that α-$Ba_3Mg_3(BO_3)_3F_3$ is a potential DUV material.

Liu *et al.* designed and synthesized KBBF-type $CsAlB_3O_6F$ crystal through flux method [56]. $CsAlB_3O_6F$ also has a KBBF-type 2D layered structure. Cs^+ is replaced by K^+, and $[BeO_3F]$ is replaced by $[AlO_3F]$. $[AlO_3F]$ and $[BO_3]$ groups are connected in the *bc* plane to form a 2D layer, and Cs^+ is located in the 18 membered ring tunnel which composed of $[AlO_3F]$ and $[BO_3]$ units (Fig. 9b). Notably, the interlaminar distance of $CsAlB_3O_6F$ (4.03 Å) is significantly smaller than that of KBBF (6.25 Å), indicating that the interlaminar force of $CsAlB_3O_6F$ is stronger than that of KBBF. Consequently, the growth characteristic of $CsAlB_3O_6F$ would be better than that of KBBF. Optical experiments show that phasematching $CsAlB_3O_6F$ has a strong SHG response ($2.0 \times$ KDP@1064 nm) and a short ultraviolet cut-off edge ($<$ 190 nm). In addition, theoretical calculation shows that the shortest second harmonic phasematching wavelength is 182 nm. All these properties indicate that $CsAlB_3O_6F$ is a potential DUV material. According to calculation of density of states, the VBs maximum of $CsAlB_3O_6F$ is mainly occupied by O 2p and F 2p orbitals, while the CBs minimum is mainly occupied by atomic orbitals of Ca 3p and B 2p.

3.1.4. $LaB_4O_6(OH)_2Cl$

Guo *et al.* designed and synthesized colorless transparent KBBF type $LaB_4O_6(OH)_2Cl$ crystal by hydrothermal method [97]. The crystal structure of $LaB_4O_6(OH)_2Cl$ is composed of 18-membered ring $[B_4O_8(OH)_2]$ structural motifs which formed by two $[BO_3(OH)]$

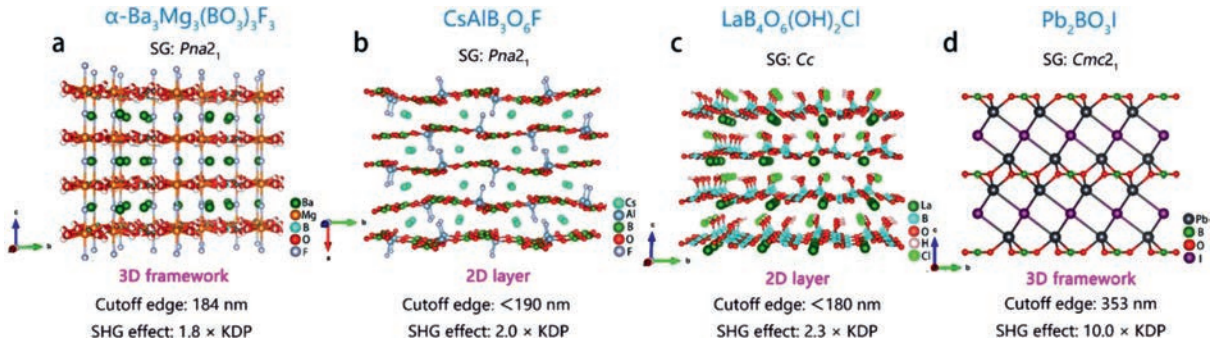

Fig. 9. Crystal structures and NLO performance of α-$Ba_3Mg_3(BO_3)_3F_3$, $CsAlB_3O_6F$, $LaB_4O_6(OH)_2Cl$ and Pb_2BO_3I.

tetrahedrons and three [BO_3] groups. These structural motifs are connected to each other to form a 2D layer (Fig. 9c). Optical experiments show that phasematching $LaB_4O_6(OH)_2Cl$ has a strong frequency doubling effect (2.3 × KDP@1064 nm) and short UV cutoff edge (< 180 nm). It can be seen from DFT calculation that the VBs maximum of $LaB_4O_6(OH)_2Cl$ are mainly determined by the atomic orbits of O 2p and Cl 3p, and the CBs minimum are predominantly composed of La 5p and B 2p orbits.

3.1.5. Pb_2BO_3I

Halasyamani and his team designed and synthesized Pb-based KBBF-type Pb_2BO_3I crystal by hydrothermal method [98]. The 3D framework crystal structure of Pb_2BO_3I is formed by [PbO_3I_2] and [BO_3] groups in *ab* plane. Compared with KBBF, the [PbO_3I_2] groups in Pb_2BO_3I replaces [BeO_3F] groups, and the K-F bond is replaced by Pb-I bond (Fig. 9d). The calculation results show that the interlayer force of Pb_2BO_3I is stronger than that of KBBF. It should be noted that Pb_2BO_3I has the strongest SHG efficiency (10.0 × KDP@1064 nm) of KBBF family NLO compounds. It shows type-I phase matching ability. Th optical experiment test proves that the ultraviolet cut-off edge of Pb_2BO_3I is 330 nm. Pb_2BO_3I has the potential to become the ultraviolet NLO materials.

3.1.6. $NH_4Be_2BO_3F_2$, γ-Be_2BO_3F, $C(NH_2)_3SO_3F$

Ye *et al.* designed and synthesized colorless and transparent KBBF-type $NH_4Be_2BO_3F_2$ and γ-Be_2BO_3F crystals by high temperature hydrothermal method [57]. $NH_4Be_2BO_3F_2$ and γ-Be_2BO_3F have similar structure with KBBF, but their interlayer force is stronger than KBBF. Especially for γ-Be_2BO_3F, the cation at A site is directly removed from its crystal structure, and the layers are directly connected by Be-F-Be bonds, which eliminates the disadvantage of KBBF layer-by-layer growth habit (Figs. 10c and d). Under 1064 nm laser irradiation, phase matching $NH_4Be_2BO_3F_2$ and γ-Be_2BO_3F have strong SHG response (1.2 and 2.3 × KDP, respectively. The ultraviolet cut-off edges of these two compounds are less than 190 nm. DFT calculation shows that their shortest second harmonic phase matching wavelengths are 173.9 nm and 146 nm, respectively. All these optical properties indicate that they have potential to become DUV NLO materials.

Recently, Ye *et al.* have grown colorless plate-like KBBF type $C(NH_2)_3SO_3F$ crystal in solution [77]. [SO_3] units replace [BO_3] units, and [SO_3F] units replace [BeO_3F] units from KBBF to $C(NH_2)_3SO_3F$. The difference is that the [BeO_3F] tetrahedrons in KBBF are arranged in opposite intervals, while the [SO_3F] groups in $C(NH_2)_3SO_3F$ are arranged in the same direction (Fig. 10b), which is in favor of the superposition of d_{ij}. $C(NH_2)_3SO_3F$ exhibits strong SHG response (5 × KDP) and moderate birefringence (0.133). The ultraviolet cut-off edge of $C(NH_2)_3SO_3F$ is 200 nm. Theoretical calculation shows that its shortest second harmonic phase matching wavelength is less than 200 nm.

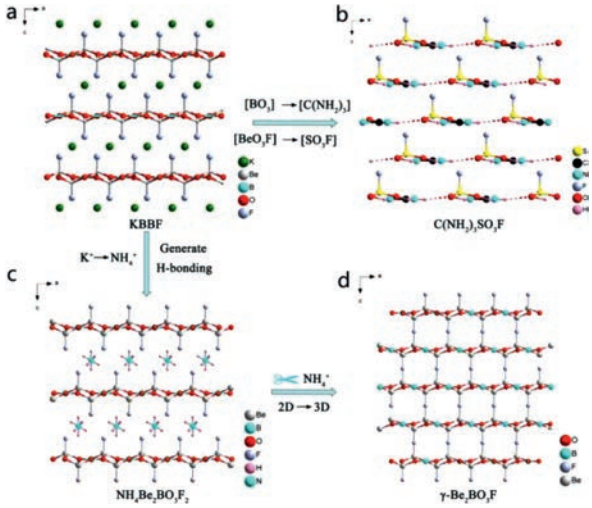

Fig. 10. Crystal structure of $NH_4Be_2BO_3F_2$, γ-Be_2BO_3F and $C(NH_2)_3SO_3F$.

In general, it is a very effective method to design DUV NLO materials using KBBF as a template. Many crystals in this part inherit the excellent properties of KBBF and overcome some intrinsic performance limitations. In the AB_4O_6F (A = Rb, Cs, Na, NH_4), $A(B_5O_7)F_3$ (A = Sr, Ca, Pb) series compounds, K^+ is replaced by other alkali metal/alkaline earth metal cations or NH_4^+, and mixed anion SBUs [BeO_3F] are replaced by [BO_3F]. These compounds exhibit a good balance among short ultraviolet cut-off edge, strong SHG response and suitable phase matching ability. In addition, the substitution of the non-toxic element B with Be and much stronger interlayer forces make these compounds more applicable in practical use. γ-Be_2BO_3F and $C(NH_2)_3SO_3F$ are potential candidate as DUV NLO materials with strong interlayer forces and excellent comprehensive properties. $Pb(B_5O_7)F_3$ and Pb_2BO_3I showed strong SHG response with 6.0 and 10.0 × KDP, respectively.

3.2. Nitrate and carbonate

In this part, the NLO crystals containing tri-coordinated groups [NO_3], [CO_3] and complex coordinated groups [MA_xB_y] are analyzed. The four compounds $Pb_2(NO_3)_2(H_2O)F_2$ [99], $Rb_3SbF_3(NO_3)_3$ [100], $KMgCO_3F$ [101] and $NaZnCO_3F$ [102] emerged in recent years are represented.

3.2.1. $Pb_2(NO_3)_2(H_2O)F_2$

Ye and his team designed and synthesized the first fluoronitrate crystal of $Pb_2(NO_3)_2(H_2O)F_2$ by hydrothermal method [103]. The 3D framework crystal structure of $Pb_2(NO_3)_2(H_2O)F_2$ consists of mixed-anion [PbO_9F_2] and [NO_3] groups (Fig. 11a). Optical experimental tests show that phasematching $Pb_2(NO_3)_2(H_2O)F_2$ has

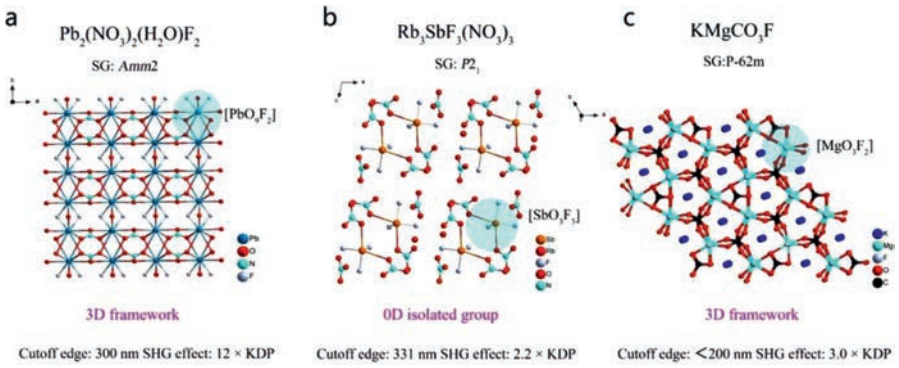

Fig. 11. Crystal structures and NLO performance of (a) $Pb_2(NO_3)_2(H_2O)F_2$, (b) $Rb_3SbF_3(NO_3)_3$ and (c) $KMgCO_3F$.

a very strong frequency doubling effect (12.0 × KDP@1064 nm) and a short ultraviolet cut-off edge (300 nm). The DFT calculation shows that the VBs maximum and CBs minimum of $Pb_2(NO_3)_2(H_2O)F_2$ are predominately determined by the atomic orbitals of O, N, Pb and F. Therefore, the linear and NLO properties of $Pb_2(NO_3)_2(H_2O)F_2$ are mainly affected by the $[NO_3]$ groups, the Pb-O and Pb-F bonds.

3.2.2. $Rb_3SbF_3(NO_3)_3$

Wang *et al.* designed and synthesized Sb-based $Rb_3SbF_3(NO_3)_3$ crystal [100]. $Rb_3SbF_3(NO_3)_3$ has a 0D isolated molecular structure, which consists of two $[SbO_3F_3]$ polyhedrons and three $[NO_3]$ groups with holes hosting Rb^+ cations (Fig. 11b). The NLO response of $Rb_3SbF_3(NO_3)_3$ is 2.2 × KDP@1064 nm, and it shows PM behavior. The bandgap of $Rb_3SbF_3(NO_3)_3$ is 3.75 eV (corresponding to 331 nm of ultraviolet cut-off edge). $Rb_3SbF_3(NO_3)_3$ has the potential to become the next generation UV NLO material. DFT calculation shows that the VBs maximum and CBs minimum of $Rb_3SbF_3(NO_3)_3$ are determined by the atomic orbitals of O, N, Sb and F, thus its optical properties are mainly affected by $[NO_3]$ and $[SbO_3F_3]$ groups.

3.2.3. $KMgCO_3F$, $NaZnCO_3F$

Halasyamani and Tran *et al.* designed and synthesized alkali metal fluorocarbonates $KMgCO_3F$ [101] and $NaZnCO_3F$ [102], respectively. They have a similar crystal structure. The crystal structure of $KMgCO_3F$ is composed of mixed anion $[MgO_3F_2]$ group and $[CO_3]$ group to form a 3D framework structure (Fig. 11c). The optical experiment test shows that both $KMgCO_3F$ and $NaZnCO_3F$ have phase matching ability and show a strong frequency doubling effect (3.0, 2.75 × KDP@1064 nm). In addition, they have short ultraviolet cut-off edges (< 180 nm, 230 nm). All these properties indicate that $KMgCO_3F$ and $NaZnCO_3F$ have the potential to become NLO materials for the next generation of UV applications.

In a word, compounds obtained by the combination of tri-coordinated groups $[NO_3]$, $[CO_3]$ and complex coordinated groups $[MA_xB_y]$ are critical for UV NLO materials exploration. All crystals of this type have good phase matching capability. $Pb_2(NO_3)_2(H_2O)F_2$ had the largest SHG effect, which was 12 × KDP. In addition, $Rb_3SbF_3(NO_3)_3$, $KMgCO_3F$ and $NaZnCO_3F$ can keep a balance between the strong SHG response and the short ultraviolet cut-off edge, and they are potential candidates for UV NLO crystals.

3.3. Phosphates

This part mainly studies the new type of NLO crystals containing *p*-block coordination tetrahedral group $[PO_4]$ and mixed anion group $[MA_xB_y]$. These compounds can be divided into the following three parts according to the combined tetrahedral units, such as $[PO_4]$, $[P_2O_7]$. The comprehensive performance, including optical band gap, SHG effect and phase matching ability, are evaluated in combination with crystal structure and complex coordinated groups arrangement ($[MA_xB_y]$ and $[PO_4]$ groups).

3.3.1. $BaZn(PO_4)F$, $RbBPO_4F$, $(NH_4)_2BPO_4F_2$

Tang *et al.* synthesized the fluorophosphate $BaZn(PO_4)F$ crystal by hydrothermal method [103]. The crystal structure of $BaZn(PO_4)F$ consists of the interconnection of $[PO_4]$ groups and $[ZnO_4F]$ mixed-anion polyhedrons to form a 3D framework structure (Fig. 12a). Optical experiments show that the ultraviolet cut-off edge of $BaZn(PO_4)F$ is less than 190 nm, and the d_{ij} is 0.26 × KDP, showing type-I PM capability. DFT calculation indicates that the VBs maximum and CBs minimum of $BaZn(PO_4)F$ are mainly determined by the atomic orbitals of Zn, P, O and F, which indicates that the effect of alkaline earth metal element Ba on its optical properties is negligible.

Subsequently, Wu *et al.* synthesized fluoroborophosphates $RbBPO_4F$ and $(NH_4)_2BPO_4F_2$ crystals by hydrothermal method [104]. In the crystal structure of $RbBPO_4F$, the mixed-anion $[BO_3F]$ and $[PO_4]$ groups are connected to each other to form a 3D tunnel structure. The alkali metal Rb^+ is located in the tunnel (Fig. 12b). As shown in Fig. 12c, the 1D chain structure of $(NH_4)_2BPO_4F_2$ is composed of $[PO_4]$ tetrahedrons and complex coordinated $[BO_2F_2]$ groups. Optical experimental tests show that the ultraviolet cut-off edges of $RbBPO_4F$ and $(NH_4)_2BPO_4F_2$ are both less than 200 nm, and their SHG effects are 0.4, 0.8 × KDP@1064 nm, respectively. $RbBPO_4F$ exhibits non-phasematching behavior due to its cubic structure, while $(NH_4)_2BPO_4F$ exhibits type-I phase matching ability. Theoretical calculations reveal that the NLO response of these two compounds mainly comes from the $[PO_4]^+$ groups.

3.3.2. $Ba_2NaP_2O_7Cl$, $CsSiP_2O_7F$, $K_2Sb(P_2O_7)F$

Chen *et al.* synthesized colorless and transparent fresnoite-like structure $Ba_2NaP_2O_7Cl$ crystal by a high temperature solid-state reaction technology [59]. $Ba_2NaP_2O_7Cl$ is a 3D tunnel structure formed by the connection of $[P_2O_7]$ dimer groups and $[NaO_4Cl_2]$ polyhedra, and Ba^{2+} is located in the center of the pore (Fig. 13a). $Ba_2NaP_2O_7Cl$ can maintain a good balance among short ultraviolet cut-off edge (< 176 nm), strong SHG response (0.9 × KDP@1064 nm), and sufficient birefringence value (0.017). All these properties indicate that $Ba_2NaP_2O_7Cl$ has the potential to be DUV NLO materials.

Ding *et al.* synthesized $CsSiP_2O_7F$ crystal by high temperature solid-state reaction technology [60]. As shown in Fig. 13b, the 3D frame structure of $CsSiP_2O_7F$ is composed of the $[P_2O_7]$ dimer unit and $[SiO_5F]$ polyhedrons, and Cs^+ are scattered in the tunnel holes. $CsSiP_2O_7F$ can also maintain a good balance between short cut-off edge (< 190 nm), strong SHG effect (0.7 × KDP@1064 nm), and good phase matching ability. DFT calculation shows that the VBs

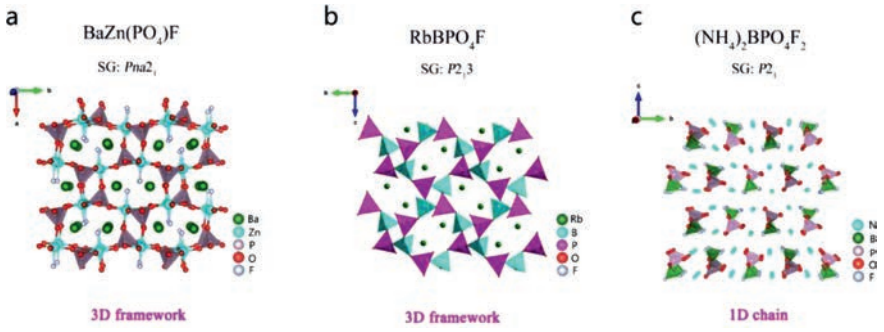

Fig. 12. Crystal structures and NLO performance of (a) $BaZn(PO_4)F$, (b) $RbBPO_4F$ and (c) $(NH_4)_2BPO_4F_2$.

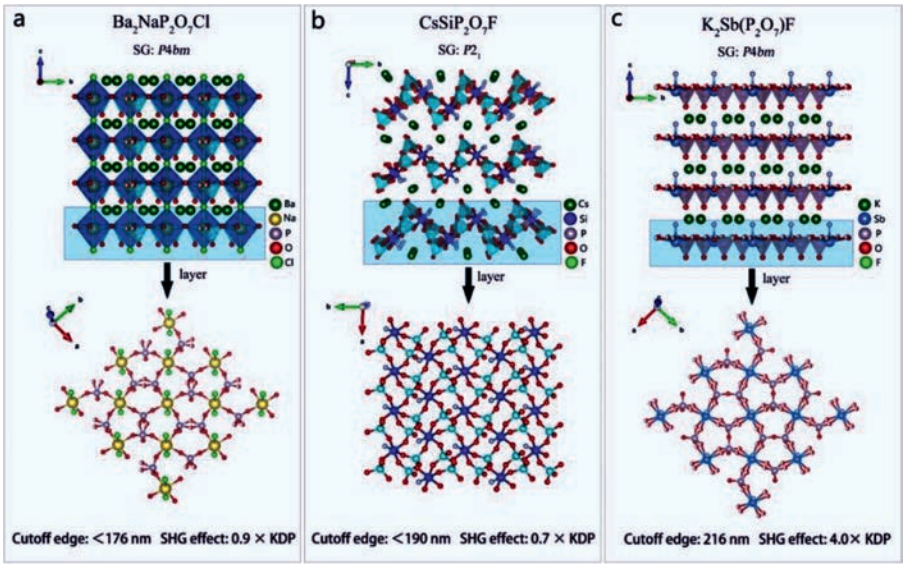

Fig. 13. Crystal structures and NLO performance of (a) $Ba_2NaP_2O_7Cl$, (b) $CsSiP_2O_7F$ and (c) $K_2Sb(P_2O_7)F$.

maximum of $CsSiP_2O_7F$ is mainly occupied by the atomic orbitals of Cs, P and Si, and the CBs minimum is occupied by the atomic orbitals of O and F, which indicates that all atoms have an effect on the linear optical properties. The SHG-density method proves that the anions $[P_2O_7]$ dimer units and $[SiO_5F]$ groups make major contributions to whole SHG effect.

Deng *et al.* synthesized colorless and transparent $K_2Sb(P_2O_7)F$ crystal by means of solvent-free synthesis technology [105]. $K_2Sb(P_2O_7)F$ has a 2D layered structure, which is built by $[P_2O_7]$ dimer and $[SbO_4F]$ polyhedra along the *ab* plane (Fig. 13c). Optical experiments show that $K_2Sb(P_2O_7)F$ has a strong frequency doubling effect (4 × KDP@1064 nm), showing the PM behavior. The ultraviolet cut-off edge of $K_2Sb(P_2O_7)F$ is 261 nm. DFT calculations show that VBs maximum of $K_2Sb(P_2O_7)F$ is mainly occupied by atomic orbitals of F, P and O, and the CBs minimum is mainly occupied by atomic orbitals of Sb and F, which indicates that the effect of alkali metal K on its optical properties is minimal.

3.3.3. $Na_3Sc_2(PO_4)_2F_3$

Xu *et al.* synthesized rare earth fluorophosphate $Na_3Sc_2(PO_4)_2F_3$ under hydrothermal conditions [106]. The 3D framework structure of $Na_3Sc_2(PO_4)_2F_3$ is composed of $[PO_4]$ tetrahedrons and $[ScO_4F_2]$ mixed-anion polyhedrons. Na^+ is scattered in the tunnel holes (Fig. 14). The SHG response of $Na_3Sc_2(PO_4)_2F_3$ is 0.26 × KDP under 1064 nm laser irradiation, and it has type-I phase matching ability. $Na_3Sc_2(PO_4)_2F_3$ exhibits short cutoff edge of 255 nm and a large birefringence value (0.0978). All these properties indicate that $Na_3Sc_2(PO_4)_2F_3$ has the potential to be a UV NLO material.

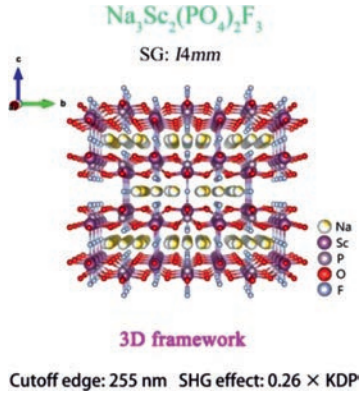

Fig. 14. Crystal structure and NLO performance of $Na_3Sc_2(PO_4)_2F_3$.

To summarize, compounds containing mixed anion groups $[MA_xB_y]$ and $[PO_4]$ are important candidates for UV/DUV NLO materials. This type of compound has strong optical anisotropy and exhibits good phase matching ability. It is worth noting that when the mixed anion groups $[MA_xB_y]$ and $[PO_4]$ are arranged in 2D layers, it is easier to maintain a balance between strong SHG response and the short ultraviolet cut-off edge. For example, $Ba_2NaP_2O_7Cl$, $CsSiP_2O_7F$, $K_2Sb(P_2O_7)F$ all show excellent comprehensive performance.

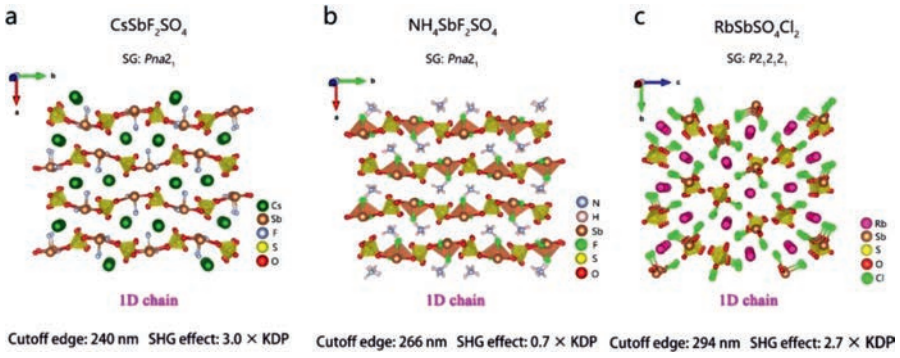

Fig. 15. Crystal structures and NLO performance of $CsSbF_2SO_4$, $NH_4SbF_2SO_4$ and $RbSbSO_4Cl_2$.

3.4. Sulfate

In addition to phosphates containing $[PO_4]$ tetrahedrons, metal sulfates are also well-known UV/DUV NLO materials. In this part, $CsSbF_2SO_4$ [107], $NH_4SbF_2SO_4$ [108] and $RbSbSO_4Cl_2$ [109] are taken as representative compounds to analyze the influence of the binding and arrangement manner of $[SO_4]$ tetra-coordination groups and mixed-anion group $[MA_xB_y]$ on optical band gap, SHG effect and phase matching ability.

3.4.1. $CsSbF_2SO_4$, $NH_4SbF_2SO_4$

Dong *et al.* designed and synthesized $CsSbF_2SO_4$ [107] by electrothermal synthesis. The 1D chain structure of $CsSbF_2SO_4$ is composed of twisted $[SbO_2F_2]$ groups and $[SO_4]$ tetrahedral groups. Cs^+ is distributed among the chains (Fig. 15a). The ultraviolet cut-off edge of $CsSbF_2SO_4$ is 240 nm. Under 1064 nm laser irradiation, it exhibits strong frequency doubling effect (3 × KDP) with phase matching behavior. The theoretical calculation indicates that the NLO response of $CsSbF_2SO_4$ mainly comes from the highly distorted $[SbO_2F_2]$ units, while the $[SO_4]$ group is beneficial to the parallel arrangement of $[SbO_2F_2]$ units.

Jantz *et al.* designed and synthesized NCS ammonia fluorine chalcogenide salt $NH_4SbF_2SO_4$ [108]. The 1D chain structure of $NH_4SbF_2SO_4$ is formed by connecting twisted $[SbO_2F_2]$ groups and $[SO_4]$ tetrahedral groups, with NH_4^+ distributed between the chains (Fig. 15b). The optical experiment test shows that the ultraviolet cut-off edge of $NH_4SbF_2SO_4$ is 266 nm. It has PM capability, and the SHG effect is about 0.7 × KDP.

3.4.2. $RbSbSO_4Cl_2$

He *et al.* synthesized $RbSbSO_4Cl_2$ by hydrothermal method [109]. $RbSbSO_4Cl_2$ has a 1D chain structure, which is composed of twisted $[SbO_3Cl_2]$ polyhedrons and $[SO_4]$ units, while Rb^+ is scattered among the chains (Fig. 15c). The ultraviolet cut-off edge of $RbSbSO_4Cl_2$ is 347 nm. Under 1064 nm laser irradiation, the frequency doubling effect is 2.7 × KDP with type-I PM capability. $RbSbSO_4Cl_2$ has the potential to become UV NLO materials. Theoretical calculations show that the VBs maximum and CBs minimum of $RbSbSO_4Cl_2$ are determined by the atomic orbitals of Rb, O, Sb, S and Cl. Therefore, the optical properties of $RbSbSO_4Cl_2$ mainly depend on $[RbO_5Cl_4]$, $[SbO_3Cl_2]$, $[SO_4]$ groups.

3.5. Complex coordinated group $[BO_3F]$ as NLO active units

$Sn[B_2O_3F_2]$: HöPPE and his team synthesized colorless massive $Sn[B_2O_3F_2]$ crystals [109]. The power X-ray diffraction test shows that $Sn[B_2O_3F_2]$ crystallizes in space group *P*31m (No. 157). The crystal structure of $Sn[B_2O_3F_2]$ is composed of two-dimensional layers connected by the $[BO_3F]$ cells along the *ab* plane, and Sn^{2+} is distributed among the layers to maintain the charge balance (Fig. 16a). The UV cutoff edge of $Sn[B_2O_3F_2]$ is 243 nm. Under 1054 nm laser irradiation, its SHG effect is even stronger that of KDP, and it has phase matching ability. $Sn[B_2O_3F_2]$ has the potential to become the next generation of UV NLO materials. Theoretical calculations show that the VBs maximum and CBs minimum of $Sn[B_2O_3F_2]$ are mainly determined by the atomic orbitals of Rb, O, Sb, S and Cl. Its optical properties mainly depend on $[RbO_5Cl_4]$, $[SbO_3Cl_2]$ and $[SO_4]$ groups.

3.6. Mixed-anion group $[TeO_2F_2]$ as NLO active units

$BaF_2TeF_2(OH)_2$: In 2020, He *et al.* designed and synthesized colorless and transparent $BaF_2TeF_2(OH)_2$ crystal by hydrothermal method [110]. Power X-ray diffraction results show that $BaF_2TeF_2(OH)_2$ belongs to NCS space group $Pmn2_1$ (No. 31). $BaF_2TeF_2(OH)_2$ has a typical aurivillius structure. The $[TeF_2(OH)_2]$ groups are connected with each other in the *ac* plane to form a two-dimensional layer, and the $[BaF_4]$ tetrahedrons are also connected by common edge to form 2D layers. The crystal structure of $BaF_2TeF_2(OH)_2$ is composed of the two layers which are mutually spaced along the *b*-axis (Fig. 16b). The UV cut-off edge of $BaF_2TeF_2(OH)_2$ is 205 nm. Under 1064 nm laser irradiation, it shows strong SHG effect (3 × KDP) and good phase matching ability. All these properties indicate that $BaF_2TeF_2(OH)_2$ has the potential to become the next generation of UV NLO materials.

3.7. Mixed-anion group $[PO_3F]$ as NLO active units

$NaNH_4PO_3F{\cdot}H_2O$: Lu *et al.* designed and synthesized colorless and transparent $NaNH_4PO_3F{\cdot}H_2O$ crystal [61]. Power x-ray diffraction results show that $NaNH_4PO_3F{\cdot}H_2O$ belongs to monoclinic space group *Pc* (No. 7). The crystal structure of $NaNH_4PO_3F{\cdot}H_2O$ is composed of $[PO_3F]$ groups, which are connected with $[NH_4]$ and H_2O molecules through hydrogen bonds, and finally form a two-dimensional layered structure, with Na^+ scattered among the layers (Fig. 16c). $NaNH_4PO_3F{\cdot}H_2O$ exhibits a strong SHG effect of 1.1 times that of KDP under 1064 nm laser irradiation. Theoretical calculation shows that its shortest second harmonic phase matching wavelength is 194 nm. There is no doubt that $NaNH_4PO_3F{\cdot}H_2O$ has the potential to apply in the next generation of DUV NLO materials.

4. Summary and outlook

To sum up, complex coordinated functional groups $[MA_xB_y]$ are excellent NLO active units, and compounds containing this group are more likely to guarantee excellent comprehensive performance. This group is combined with traditional NLO active group ($[MQ_4]$ (M = metal cationic, Q = S, Se, Te, P), $[IO_3]$, $[SeO_3]$, $[TeO_3]$, $[CO_3]$, $[NO_3]$, $[SO_4]$, $[PO_4]$, B-O groups, *etc.*) is an important direction

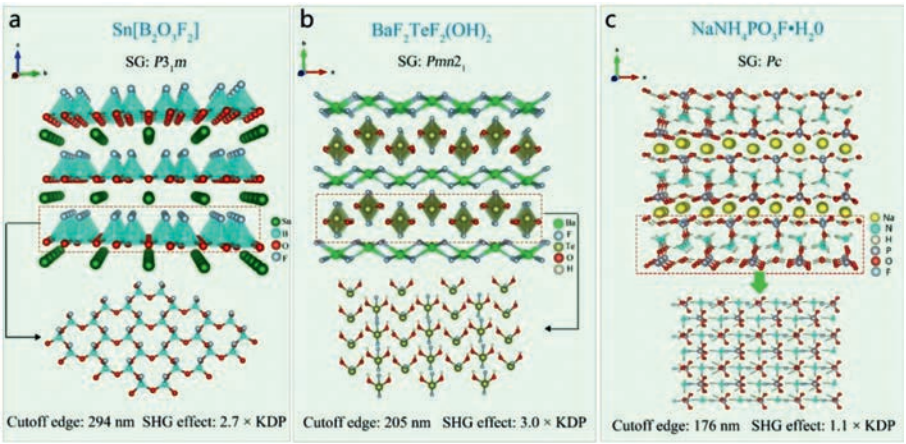

Fig. 16. Crystal structures and NLO performance of $Sn[B_2O_3F_2]$, $NaNH_4PO_3F{\cdot}H_2O$ and $BaF_2TeF_2(OH)_2$.

to explore new high-performance nonlinear optical materials. In this paper, a comprehensive review of NLO crystal materials with mixed anion functional groups $[MA_xB_y]$ as the basic structural unit is made based on theoretical analysis results, anion combination methods, and available experimental performance test results. Through systematic summary, it can be concluded that: (1) The combination of complex coordinated groups $[MA_xB_y]$ and $[C(1)O_3]$ (C(1) = I, Se, Te) oxygen-containing groups is conducive to the synthesis of large band gap mid-IR NLO crystals with good phase matching ability. In order to solve the shortcoming of small NLO effect of this kind of compound, it is necessary to introduce d^0-transition metal element, *e.g.*, W^{6+}, V^{5+}, or metal element containing stereochemically active lone pairs, which is easy to produce strong distorted multi-coordination groups *e.g.*, Bi and Pb. (2) The combination of the complex coordinated groups $[MA_xB_y]$ and $[MQ_4]$ (Q = S, P) tetra-coordinated units to form a 3D frame structure is conducive to the synthesis of ideal MIR NLO crystals with phase matching ability, large band gap and strong SHG effect. (3) The comprehensive performance of IR NLO crystals with complex coordinated groups $[MA_xB_y]$ as SBUs is improved compared with that of traditional single anionic compounds. (4) When the mixed anion functional groups $[MO_xF_{4-x}]$ and $[C(2)O_3]$ (C(2) = B, N, C) tri-coordinated oxygen-containing groups are arranged in a KBBF-like structure model (three coordination groups and four coordination groups containing halogen F are connected to form a 2D layer), it is beneficial to the formation of excellent deep ultraviolet NLO crystals (short ultraviolet cut-off edge, strong SHG effect, small second harmonic phasematching wavelength). (5) When the complex coordinated functional groups $[MA_xB_y]$ and $[C(3)O_4]$ (C(3) = P, S) tetra-coordination groups are arranged in 2D layers, and there are scattered alkali/alkaline earth metal cations in the structure, it is more likely to achieve a balance between short cut-off edge and strong SHG effect. (6) UV/DUV NLO crystals composed of a 2D layered arrangement of complex coordinated groups $[MA_xB_y]$ exhibit excellent comprehensive properties. It is believed that the combination mode of the anion NLO active units and the regulation of the arrangement rules on the optical properties above will be of guiding significance for the future design of MIR/DUV NLO materials.

For the future design and synthesis of complex coordinated NLO crystals, we should focus on the following aspects: (1) For the field of IR nonlinear optics, the research of tetra-coordinated compounds is relatively less, and we should pay more attention to the diamond-like compounds composed of $[MA_xB_{4-x}]$ (A, B is one of the elements of P, O, S, Se, F, Cl, Br, I) with four coordination groups arranged in parallel. (2) For the field of UV/deep UV nonlinear optics, more alternative structural templates similar to KBBF should be explored. In addition, at present, there are only a few compounds in type IV NLO materials with only $[MA_xB_{4-x}]$ as SBUs, which has a lot of exploration potential in the future. (3) The practical application of NLO materials needs large single crystals with good quality, so the best growth conditions of NLO crystals with mixed anion group $[MA_xB_y]$ as SBUs should be explored in the future. (4) The design and synthesis of $[MA_xB_{4-x}]$ as SBUs NLO crystal is a time-consuming and laborious work. In order to improve the efficiency, it is necessary to combine theoretical analysis with experimental exploration.

Declaration of competing interest

The authors declare no conflict of interest.

Acknowledgment

This work was supported by National Natural Science Foundation of China (No. 51972208).

References

[1] N. Yoshikawa, T. Tamaya, K. Tanaka, Science 356 (2017) 736–738.
[2] L. Kang, F. Liang, X. Jiang, Z. Lin, C. Chen, Acc. Chem. Res. 53 (2020) 209–217.
[3] P. Becker, Adv. Mater. 10 (1998) 979–992.
[4] H. Lu, R. Gautier, M.D. Donakowski, et al., J. Am. Chem. Soc. 135 (2013) 11942–11950.
[5] N.L.B. Sayson, T. Bi, V. Ng, et al., Nat. Photonics 13 (2019) 701.
[6] J. Zhao, D.J. Mei, W.K. Wang, Y.D. Wu, D.F. Xue, J. Rare Earth 39 (2021) 1455–1466.
[7] S.P. Guo, X. Cheng, Z.D. Sun, et al., Angew. Chem. Int. Ed. 58 (2019) 8087–8091.
[8] W. Cao, D. Mei, Y. Yang, et al., Chem. Commun. 55 (2019) 14510–14513.
[9] S.P. Guo, Y. Chi, H.G. Xue, Angew. Chem. Int. Ed. 57 (2018) 11540–11543.
[10] C. Yang, X. Liu, C. Teng, et al., Mater. Today Phys. 19 (2021) 100432.
[11] Y. Zhou, Q.G. Ding, Y.C. Liu, et al., Chin. Chem. Lett. 32 (2021) 263–265.
[12] F.J. Hou, D.J. Mei, W.K. Wang, Y.D. Wu, J. Synth. Cryst. 49 (2020) 1427–1442.
[13] Y.Y. Xue, X.D. Xu, L.B. Su, J. Xu, J. Synth. Cryst. 49 (2020) 1347–1360.
[14] Z.T. Lu, S.P. Guo, J. Synth. Cryst. 49 (2020) 1443–1456.
[15] P.A. Franken, A.E. Hall, C.W. Peters, G. Weinreich, Phys. Rev. Lett. 7 (1961) 118–120.
[16] C.T. Chen, B.C. Wu, A.D. Jiang, G.M. You, Sci. Sin. Ser. B 28 (1985) 235–243.
[17] C.T. Chen, Y.C. Wu, A.D. Jiang, et al., J. Opt. Soc. Am. B 6 (1989) 616–621.
[18] G.D. Boyd, R.C. Miller, K. Nassau, W.L. Bond, A. Savage, Appl. Phys. Lett. 5 (1964) 234–236.
[19] J.J. De Yoreo, A.K. Burnham, P.K. Whitman, Int. Mater. Rev. 47 (2002) 113–152.
[20] J.D. Bierlein, H. Vanherzeele, J. Opt. Soc. Am. B 6 (1989) 622–633.
[21] S.P. Guo, Y. Chi, G.C. Guo, Coord. Chem. Rev. 335 (2017) 44–57.
[22] L. Song, C.L. Hu, X. Xu, F. Kong, J.G. Mao, Angew. Chem. Int. Ed. 54 (2015) 3679–3682.
[23] Y. Wang, S. Pan, Coord. Chem. Rev. 323 (2016) 15–35.

[24] C. Wu, G. Yang, M.G. Humphrey, C. Zhang, Coord. Chem. Rev. 375 (2018) 459–488.
[25] J. Zhao, D. Mei, Y. Yang, et al., Inorg. Chem. 58 (2019) 15029–15033.
[26] I. Chung, M.G. Kanatzidis, Chem. Mater. 26 (2014) 849–869.
[27] M. Mutailipu, M. Zhang, Z. Yang, S. Pan, Acc. Chem. Res. 52 (2019) 791–801.
[28] X.M. Jiang, S.J. Lin, C. He, B.W. Liu, G.C. Guo, Angew. Chem. Int. Ed. 60 (2021) 11799–11803.
[29] D. Mei, W. Cao, N. Wang, et al., Mater. Horiz. 8 (2021) 2330–2334.
[30] B.L. Wu, C.L. Hu, F.F. Mao, R.L. Tang, J.G. Mao, J. Am. Chem. Soc. 141 (2019) 10188–10192.
[31] H. Yu, W. Zhang, J. Young, J.M. Rondinelli, P.S. Halasyamani, Adv. Mater. 27 (2015) 7380.
[32] X. Wang, Y. Wang, B. Zhang, et al., Angew. Chem. Int. Ed. 56 (2017) 14119–14123.
[33] S. Zhao, P. Gong, S. Luo, et al., J. Am. Chem. Soc. 136 (2014) 8560–8563.
[34] C. Jin, X. Shi, H. Zeng, et al., Angew. Chem. 133 (2021) 20632–20638.
[35] R.A. Li, Z. Zhou, Y.K. Lian, et al., Angew. Chem. Int. Ed. 59 (2020) 11861–11865.
[36] C. Chen, Y. Wu, R. Li, Int. Rev. Phys. Chem. 8 (1989) 65–91.
[37] G.C. Guo, Y.G. Yao, K.C. Wu, L. Wu, J.S. Huang, Prog. Chem. 13 (2001) 151–155.
[38] J. Mark, J. Wang, K. Wu, et al., J. Am. Chem. Soc. 141 (2019) 11976–11983.
[39] Y. Pan, S.P. Guo, B.W. Liu, H.G. Xue, G.C. Guo, Coord. Chem. Rev. 374 (2018) 464–496.
[40] Y.Y. Li, W.J. Wang, H. Wang, H. Lin, L.M. Wu, Cryst. Growth Des. 19 (2019) 4172–4192.
[41] B.W. Liu, H.Y. Zeng, X.M. Jiang, et al., Chem. Sci. 7 (2016) 6273–6277.
[42] C. Wu, X.X. Jiang, Z.J. Wang, et al., Angew. Chem. 133 (2021) 3506–3510.
[43] H. Kageyama, K. Hayashi, K. Maeda, et al., Nat. Commun. 9 (2018) 772.
[44] B.W. Liu, X.M. Jiang, G.E. Wang, et al., Chem. Mater. 27 (2015) 8189–8192.
[45] M.Y. Ran, Z.J. Ma, H. Chen, et al., Chem. Mater. 32 (2020) 5890–5896.
[46] R.Q. Wang, F. Liang, F.K. Wang, et al., Angew. Chem. Int. Ed. 58 (2019) 8078–8081.
[47] C.T. Chen, Y.N. Xia, D.Y. Tang, B.C. Wu, Adv. Mater. 7 (1995) 79–81.
[48] D. Cyranoski, Nature 457 (2009) 953–955.
[49] Y. Wang, B.B. Zhang, Z.H. Yang, S.L. Pan, Angew. Chem. Int. Ed. 57 (2018) 2150–2154.
[50] Z. Zhang, Y. Wang, B. Zhang, Z. Yang, S. Pan, Angew. Chem. Int. Ed. 57 (2018) 6577–6581.
[51] G. Shi, Y. Wang, F. Zhan, et al., J. Am. Chem. Soc. 139 (2017) 10645–10648.
[52] M. Mutailipu, M. Zhang, B. Zhang, et al., Angew. Chem. Int. Ed. 57 (2018) 6095–6099.
[53] S. Han, M. Mutailipu, A. Tudi, Z. Yang, S. Pan, Chem. Mater. 32 (2020) 2172–2179.
[54] Z. Zhang, Y. Wang, B. Zhang, Z. Yang, S. Pan, Inorg. Chem. 57 (2018) 4820–4823.
[55] M. Mutailipu, M. Zhang, H. Wu, et al., Nat. Commun. 9 (2018) 3089.
[56] H.K. Liu, Y. Wang, B.B. Zhang, Z.H. Yang, S.L. Pan, Chem. Sci. 11 (2020) 694–698.
[57] G. Peng, N. Ye, Z.S. Lin, et al., Angew. Chem. Int. Ed. 57 (2018) 8968–8972.
[58] M. Luo, C.S. Lin, D.H. Lin, N. Ye, Angew. Chem. Int. Ed. 59 (2020) 15978–15981.
[59] J. Chen, L. Xiong, L. Chen, L.M. Wu, J. Am. Chem. Soc. 140 (2018) 14082–14086.
[60] Q. Ding, X. Liu, S. Zhao, et al., J. Am. Chem. Soc. 142 (2020) 6472–6476.
[61] J. Lu, J.N. Yue, L. Xiong, et al., J. Am. Chem. Soc. 141 (2019) 8093–8097.
[62] C. Wu, L. Lin, X.X. Jiang, et al., Chem. Mater. 31 (2019) 10100–10108.
[63] F.F. Mao, C.L. Hu, X. Xu, et al., Angew. Chem. Int. Ed. 56 (2017) 2151–2155.
[64] H. Fan, C. Lin, K. Chen, et al., Angew. Chem. Int. Ed. 59 (2020) 5268–5272.
[65] J. Chen, C.L. Hu, X.H. Zhang, et al., Angew. Chem. Int. Ed. 59 (2020) 5381–5384.
[66] S.S. Shi, C.S. Lin, G.S. Yang, et al., Chem. Mater. 32 (2020) 7958–7964.
[67] F.G. You, F. Liang, Q. Huang, et al., J. Am. Chem. Soc. 141 (2019) 748–752.
[68] X.L. Chen, H. Jo, K.M. Ok, Angew. Chem. Int. Ed. 59 (2020) 7514–7520.
[69] J. Chen, C. Lin, D. Zhao, et al., Angew. Chem. Int. Ed. 59 (2020) 23549–23553.
[70] X.M. Liu, P.F. Gong, Y. Yang, G.M. Song, Z.S. Lin, Coord. Chem. Rev. 400 (2019) 213045.
[71] M. Mutailipu, K.R. Poeppelmeier, S. Pan, Chem. Rev. 121 (2021) 1130–1202.
[72] F.J. Hou, D.J. Mei, M.J. Xia, Y.D. Wu, Coord. Chem. Rev. (2021) 214038.
[73] W.K. Wang, D.J. Mei, F. Liang, et al., Coord. Chem. Rev. 421 (2020) 213444.
[74] C.L. Hu, J.G. Mao, Coord. Chem. Rev. 288 (2015) 1–17.
[75] J. Chen, C.L. Hu, F.F. Mao, J.H. Feng, J.G. Mao, Angew. Chem. Int. Ed. 58 (2019) 2098–2102.
[76] H. Yu, M.L. Nisbet, K.R. Poeppelmeier, J. Am. Chem. Soc. 140 (2018) 8868–8876.
[77] M. Luo, F. Liang, X. Hao, et al., Chem. Mater. 32 (2020) 2615–2620.
[78] M. Zhang, X. Su, M. Mutailipu, Z.H. Yang, S.L. Pan, Chem. Mater. 29 (2017) 945–949.
[79] T. Abudouwufu, M. Zhang, S. Cheng, Z. Yang, S. Pan, Chem. Eur. J. 25 (2019) 1221–1226.
[80] L. Cao, M. Luo, C. Lin, et al., Chem. Commun. 56 (2020) 10734–10737.
[81] G. Peng, Y. Yang, T. Yan, et al., Chem. Sci. 11 (2020) 7396–7400.
[82] M.L. Liang, Y.X. Ma, C.L. Hu, F. Kong, J.G. Mao, Chem. Mater. 32 (2020) 9688–9695.
[83] J.Y. Chung, H. Jo, S. Yeon, et al., Chem. Mater. 32 (2020) 7318–7326.
[84] H.K. Zhao, P.F. Gong, X.Y. Zhang, et al., Dalton Trans. 49 (2020) 14046–14051.
[85] C. Wu, X.X. Jiang, L. Lin, et al., Chem. Mater. 32 (2020) 6906–6915.
[86] C. Wu, L. Li, L. Lin, et al., Chem. Mater. 32 (2020) 3043–3053.
[87] Y.X. Ma, C.L. Hu, B.X. Li, F. Kong, J.G. Mao, Inorg. Chem. 57 (2018) 11839–11846.
[88] X. Wang, X. Jiang, H. Liu, et al., Dalton Trans. 47 (2018) 1911–1917.
[89] R.Q. Wang, Y.W. Guo, X. Zhang, et al., Inorg. Chem. 59 (2020) 9944–9950.
[90] X. Chen, K.M. Ok, Chem. Asian J. 15 (2020) 3709–3716.
[91] X. Chen, Q. Jing, K.M. Ok, Angew. Chem. Int. Ed. 59 (2020) 20323–20327.
[92] Y. Tsujimoto, C.A. Juillerat, W. Zhang, et al., Chem. Mater. 30 (2018) 6486–6493.
[93] W. Xing, P. Fang, N. Wang, et al., Inorg. Chem. 59 (2020) 16716–16724.
[94] Y.C. Liu, Y.G. Shen, S.G. Zhao, J.H. Luo, Coord. Chem. Rev. 407 (2020) 213152.
[95] J. Dang, D. Mei, Y. Wu, Z. Lin, Coord. Chem. Rev. 431 (2021) 213692.
[96] F. Yang, L. Wang, L. Huang, G.H. Zou, Coord. Chem. Rev. 423 (2020) 213491.
[97] F. Guo, J. Han, J. Cheng, et al., Inorg. Chem. 57 (2018) 14953–14960.
[98] H. Yu, N.Z. Koocher, J.M. Rondinelli, P.S. Halasyamani, Angew. Chem. Int. Ed. 57 (2018) 6100–6103.
[99] G. Peng, Y. Yang, Y.H. Tang, et al., Chem. Commun. 53 (2017) 9398–9401.
[100] L. Wang, F. Yang, X. Zhao, et al., Dalton Trans. 48 (2019) 15144–15150.
[101] T.T. Tran, J. Young, J.M. Rondinelli, P.S. Halasyamani, J. Am. Chem. Soc. 139 (2017) 1285–1295.
[102] G. Peng, Y.H. Tang, C.S. Lin, et al., J. Mater. Chem. C 6 (2018) 6526–6533.
[103] X.Y. Tang, J.X. Mi, R.C. Zhuang, et al., Inorg. Chem. 58 (2019) 4508–4514.
[104] B. Wu, C. Hu, R. Tang, et al., Inorg. Chem. Front. 6 (2019) 723–730.
[105] Y.L. Deng, L. Huang, X.H. Dong, et al., Angew. Chem. Int. Ed. 59 (2020) 21151–21156.
[106] F. Xu, G. Peng, C. Lin, et al., J. Mater. Chem. C 8 (2020) 4965–4972.
[107] X. Dong, L. Huang, C. Hu, et al., Angew. Chem. Int. Ed. 58 (2019) 6528–6534.
[108] S.G. Jantz, M. Dialer, L. Bayarjargal, et al., Adv. Opt. Mater. 6 (2018) 1800497.
[109] F. He, Y. Deng, X. Zhao, et al., J. Mater. Chem. C 7 (2019) 5748–5754.
[110] F. He, Y. Ge, X. Zhao, et al., Dalton Trans. 49 (2020) 5276–5282.